DIFFUSION TENSOR FIBER TRACKING WITH SELF-ORGANIZING FEATURE MAPS

by

Dilek Göksel Duru

B.Sc. in Physics Engineering, Istanbul Technical University, 1999

M.Sc. in Biomedical Engineering, Boğazici University, 2002

Submitted to the Institute of Biomedical Engineering

in partial fulfillment of the requirements

for the degree of

Doctor

of

Philosophy

Boğaziçi University

2013

DIFFUSION TENSOR FIBER TRACKING WITH SELF-ORGANIZING FEATURE MAPS

APPROVED BY:

Prof.Dr. Mehmed Özkan (Thesis Advisor)	.....
Prof.Dr. Ahmet Ademoğlu	.....
Prof.Dr. Tamer Demiralp	.....
Assoc.Prof.Dr. Aziz M. Uluğ	.....
Assoc.Prof.Dr. Burak Acar	.....

DATE OF APPROVAL: 7 June 2013

ACKNOWLEDGMENTS

First of all, I would like to express special thanks to my advisor Prof. Dr. Mehmed Özkan for his supervision, encouragement, and support, and for giving me the freedom in choosing Diffusion MRI as the course of my research at the very beginning, which I now realize would have been allowed by very few professors.

I would also like to express my deep thanks to Assoc. Prof. Aziz M. Uluğ for reviewing the rough draft of the thesis, and for his suggestions and helpful comments.

I would also like to thank the members of the committee Assoc. Prof. Burak Acar, Prof. Dr. Tamer Demiralp and Prof. Dr. Ahmet Ademoğlu for their time and attention.

I would like to thank Prof. Dr. Ahmet Ademoğlu for his valuable comments to improve my latest manuscript. I am grateful to him for his insightful comments and discussions on my research.

I am also grateful to Prof. Dr. Derek K. Jones at Cardiff University and Dr. Stefan Skare at Stanford University for providing brain data at the beginning of the study and for their insightful comments.

It was great to be a part of the Institute of Biomedical Engineering as a full time research and teaching assistant throughout my graduate years. I am grateful for the opportunities served in there during my course of study and research. Especially I would like to express my gratitude to Prof. Dr. Yekta Ülgen, the Director of the Institute, also for his valuable comments and suggestions about my latest manuscript.

I would also like to thank the Institute's Administrative Secretary Mrs. Çiğdem Günsür Çelik, my dear friend for her friendship and all the encouragement in various

ways through all these years.

I would also express my special thanks to Oya Özdoğan, Mustafa Cevizbaş and Seyfi Berk at Boğaziçi University Library, and Muhammed Avşar at Institute's Secretarait for being so kind and helpful all times.

Any word and expression would be deficient, anyway I would like to express my deep feelings for my beloved and precious ones. I would eternally like to thank my parents for their neverending support and encouragement, not only over my PhD years, but also throughout my whole life. I would like to express special thanks to my dearest family Asuman and Metin Göksel, whose moral support and patience have made this work possible. I would like to express my immense gratitude to them for giving me liberty in any decision of my life, and for enabling me a favorable environment, and the education I desired, without which I could not have been so far. This thesis is dedicated to them and to the loving memory of my grandmom Faika Özdeniz, my maternal uncle Suavi Özdeniz, who passed away untimely, Nazife Göksel and my hundred years old grandpa Nurettin Göksel, requiescant in pace.

And my dearest, beloved soulmate Deniz, I really can't express my gratitude to him. I would like to acknowledge the worthy discussions we had related to my research. Besides his valuable and helpful suggestions, he's always been supportive, compassionate and understanding. He sure made life much easier and delighted for me ever since he joined my life.

Last, but not least, many thanks go to all my dearest friends and acquaintances at home and abroad for their love and support, for listening to me, and for believing in me.

ABSTRACT

DIFFUSION TENSOR FIBER TRACKING WITH SELF-ORGANIZING FEATURE MAPS

The diffusion tensor imaging (DTI) is unique in its ability to estimate the white matter (WM) fiber tracts in vivo noninvasively. The post-processing of DT images needs proper image analysis and visualization tools. However, accurate WM anatomical maps should be provided to clarify the multiple orientational fiber paths within uncertainty regions. These regions with intersecting trajectories generate a critical tractography issue in DTI literature. WM fiber tractography needs a standardization, a generally accepted fiber tract atlas which is the main concern of the various research groups in the field. In this thesis, the special class of artificial neural networks (ANN) namely Kohonen's self organizing feature maps (SOFMs) is proposed for the analysis of DT images. This SOM based tractography approach called SOFMAT (Self-Organizing Feature Mapping Tractography) relies on unsupervised learning method for the mapping of high dimensional data into a 1D, 2D, or higher dimensional data space depending on the topological ordering constraint. The unsupervised approach enables SOFMAT to order the principal diffusivity of the fibers in the DTI into neural pathways. A major advantage of the topological maps produced by SOFMAT is that it retains the underlying structure of the input space, while the dimensionality of the input space is reduced. As a result, an artificial neuronal map is obtained with weights encoding the stationary probability density function of the input pattern vectors. Building fiber tracking maps based on the diffusion tensor information which learn through self organization in a neurobiologically aspect is the aim of the study. SOFMAT has been tested to reveal uncertainties in fiber tracking. A well known artificial dataset called PISTE was used to access the capabilities of SOFMAT. After identifying an affective configuration, SOFMAT was employed for human tractography.

Keywords: DTI, Tensor, Anisotropy, Fiber Tractography, Self-Organizing Maps.

ÖZET

ÖZDÜZENLEYİCİ HARİTALAR İLE DİFÜZYON TENSÖR YOLAK TAKİBİ

Difüzyon tensör görüntüleme, in vivo ak madde yolaklarını noninvasif olarak tahmin edebilme özelliği ile tektir. DT imgelerinin işlenmesi için uygun imge işleme ve görselleştirme araçlarına gerek duyulmaktadır. Ancak, belirsizlik bölgelerindeki çoklu yön içeren yolakların saptanabilmesi için uygun ak madde anatomik haritaları gerekmektedir. Kesişen yolak geometrileri içeren bu bölgeler DTG literatüründe kritik bir traktografi sorunu yaratmaktadır. Ak madde traktografisi standartlaşmayı ve genel olarak bu alanda çalışan pek çok araştırma grubunun ana ilgi alanı olan, kabul edilmiş yolak takip atlası saptanmasını gerektirmektedir. Bu tezde, yapay sinir ağlarının özel bir biçimi olan Kohonen özdüzenleyici haritaları, DT imgelerini analiz etmek amaçlı önerilmiştir. Özdüzenleyici haritaları tabanlı traktografi yaklaşımı SOFMAT (Özdüzenleyici Haritalama Traktografisi) gözetimsiz öğrenmeye dayalıdır ve yüksek boyutlu verinin topolojik sıralama kısıtına bağlı olarak 1B, 2B veya daha yüksek boyutta veri uzayına haritalanmasıdır. Gözetimsiz yaklaşım, SOFMAT'ın DTG'de yolaklara ait birincil difüzivitenin nöral yollar şeklinde düzenlemesine imkan sağlar. SOFMAT' ın sonucu topolojik haritaların önemli bir avantajı, girdi uzayının boyutu azaltılırken, girdi uzayının altında kalan yapıya sadık kalması ve korumasıdır. Sonuç olarak, girdi vektör desenini yansıtan olasılık yoğunluğu fonksiyonunu ifade eden ağırlıklarla bir yapay nöron haritası elde edilmektedir. Nörobiyolojik yaklaşımla, özdüzenleyici haritalarla öğrenen DT bilgisine dayalı yolak takip haritaları oluşturulması çalışmanın amacını oluşturmaktadır. Yapay sinir ağları mantığına dayalı bu yaklaşım yolak traktografisindeki belirsizlikleri çözümlemek için denenmiştir. PISTE isimli yapay veri seti SOFMAT'ın kapasitesini ölçmek için kullanılmıştır. Etkili bir konfigürasyon saptanması sonrasında, SOFMAT insan beyin traktografisine uygulanmıştır.

Anahtar Sözcükler: DTG, Tensör, Anizotropi, Traktografi, Özdüzenleyici haritalar.

TABLE OF CONTENTS

LIST OF FIGURES

LIST OF TABLES

LIST OF SYMBOLS

M^+	Transverse magnetization
$\vec{B_0}$	Homogenous magnetic field
D	Diffusion tensor
$\vec{G}$	Magnetic gradient pulse vector
$\S_i$	Signal received with the i diffusion gradient pulse
b	Diffusion weighting factor
$\|g_i\|$	Strength of the ith diffusion gradient pulse
$\hat{g}_i$	ith diffusion gradient vector
w_{ij}	Weight vector of the jth node
h_{ij}	Topological neighborhood
d_{ij}	Euclidean distance
λ_1	Principal diffusion vector
λ_2	Secondary diffusion vector
λ_3	Tertiary diffusion vector
δ_{ij}	Kronecker delta
$\phi(x)$	Phase distribution in space
Δ	Duration
γ	Gyromagnetic ratio
η	Learning rate

LIST OF ABBREVIATIONS

DTI	Diffusion Tensor Imaging
WM	White Matter
SOFM	Self-Organizing Feature Mapping
SOFMAT	Self-Organizing Feature MAp Tractography
DTT	Diffusion Tensor Tractography
MRI	Magnetic Resonance Imaging
NMR	Nuclear Magnetic Resonance
PISTE	Phantom Images for Simulating Tractography Errors
PCA	Principal Component Analysis
FA	Fractional Anisotropy
ANN	Artificial Neural Networks
SNR	Signal to Noise Ratio
PDD	Principal Diffusivity Direction
PDF	Probability Density Function

1. INTRODUCTION

Diffusion tensor imaging (DTI) is a unique modality providing invasive fiber track pathway information non-invasively [1–3]. The brain tracts' orientation and quantity estimation is of great importance in defining the architecture and pathology of myelinated axonal white matter fibers. The accuracy of white matter (WM) anatomical maps obtained by DTI is uncertain [4, 5], an inherent problem in diffusion tensor fiber tractography. There is still a need for improved image analysis, standardized fiber tractography and visualization tools [4–6]. Accurate WM anatomical maps should be provided to clarify the multiple orientational fiber paths within uncertainty regions. Intersecting trajectories like crossing, kissing, branching fibers create the uncertainty regions within a voxel, and generate a critical tracking problem in DTI literature and further research is required. To overcome the critical tracking problem in the uncertainty regions, artificial neural network class namely Kohonen's Self-Organizing Feature Mapping (SOFM, SOM) is proposed in this thesis. The proposed SOM based tractography approach, called SOFMAT (Self Organizing Feature Mapping Tractography) relies on unsupervised learning for the mapping of six dimensional DT data into a 3D connectivity map based on the topological ordering constraint [7]. The unsupervised approach identifies a likely output corresponding to the input data. Self learning process takes place through weight update in each iteration, and the output units self-organize by competing to represent the input data pattern [8]. This assumption enables SOFMAT to connect input vectors defining the principal diffusivity of the fibers in the DTI into strings. As a result, a neuron map is obtained with weights encoding the stationary probability density function of the input pattern vectors [7]. Creating fiber tractography maps upon diffusion tensor images based on the neurobiological aspect of learning through self organization is an inspiration of the proposed study.

1.1 Motivation

Tractography is an user dependent technique, where the user should possess great knowledge about neuroanatomy. There isn't any gold standard and any generalized fiber tract atlas, yet. The details and the limitations of diffusion tensor imaging and tractography are given in detail in Chapter 2.1.6. The information about the white matter (WM) anatomical maps derived by diffusion tensor tractography (DTT) need validation. The drawback here is the general inability of the diffusion tensor analyzing methods in describing branching axonal structures and crossing fibers. These multiple orientational maxima within a single voxel lead to the uncertainty problem in DT literature [4,6]. Our proposed tool aims to tackle the uncertainty problem benefiting from the complimentary probabilities of the neurons forming a string.

1.2 Organization of this Manuscript

The sections of this dissertation are organized as follows:

The first Chapter is the Introduction, and presents the motivation and original contributions of the study.

Chapter 2 provides background information: the mathematics of tensor valued data, the basic physics of diffusion and diffusion imaging, and most importantly, a through description of tensor shape. The classical Kohonen's SOM is introduced in Background. Also the common diffusion tensor resource named PISTE (Phantom Images for Simulating Tractography Errors) which is used for benchmarking the accuracy and acceptability of the proposed approach is given in detail in Chapter 2.

The methodology is explained in Chapter 3. This chapter ties the mathematical description of tensor shape with the biological and anatomical significance of shape in DTI scans together, and presents the two novel diffusion tensor tracking methodology,

which are the main focus of this dissertation. The methodology chapter is followed by Chapter 4, the Results. The Results are discussed in two subsections namely the Experimental Scenarios and Targets, and the Human Data.

The Results are discussed in Chapter 5. Finally, the dissertation is concluded with Conclusion and Future Work in Chapter 6.

1.3 Original Contributions

The most significant original contribution of this thesis is the development of a white matter fiber tracking method based on artificial neural networks. Artificial neural nets' learning algorithms are already accepted in the literature in brain and neuroscientific researches. Relying on the citation reports, unsupervised learning algorithm is proposed in order to analyze diffusion tensor eigensystem and to handle the fiber tracking problem for the first time. Another contribution is the ability of the method to provide more info in the selected region of interest and to resolve multiple fiber tracks within uncertainty regions, curved trajectories and define a weighted fiber path (Chapter 3.3-3.6).

The proposed method and its implementation presented in this thesis were collected in a framework named SOFMAT. The algorithms developed in Matlab environment contributed to this framework unifying a of state-of-the-art algorithm dedicated to diffusion tensor image processing. The possible applications of diffusion tensor imaging are growing, and analysis of tensor data is an active area of recent research.

In my research, I focused on the development of a new diffusion tensor fiber tracking algorithm. My main research area concentrates on fiber tracking algorithm based on artificial neural networks specifically self organizing feature maps. As a side research, while researching the correct implementation of SOM into DTI analysis, a routine computer vision method namely stack linked list methodology is also implemented on diffusion tensor eigenvectors. The SOFMAT technique consists of three

major steps:

- The simulation of the algorithm on artificial data to test, verify and evaluate the SOFMAT routine.
- The construction of the SOFMAT maps from the simulation data.
- And finally, the actual tract reconstruction on real data.

SOFMAT is able to continue tracking in regions of fiber crossing such as crossing, kissing, and spiral which contain more than one fiber direction. The commonly used streamline tracking methods are not efficient to track these regions as will be explained in detail in Chapter 4 and 5, and result false reconstructions or aborted tracts. SOFMAT is also able to reconstruct curving tracts that cannot be reconstructed by the streamline techniques. A comparison of the results of SOFMAT algorithm with streamline reconstructions is given in Chapter 4 to illustrate the advantages of the proposed tracking method presented in this study.

2. Background

2.1 Diffusion Tensor Imaging

2.1.1 From Diffusion Coefficient to Diffusion Tensor

Diffusion is also called random motion, Brownian motion or intra-voxel incoherent motion. It is the random motion of molecules due to thermal energy. Hänggi and Marchesoni give a nice introduction to the history of Brownian motion in [9]. Brownian motion was first observed by Robert Brown in 1828 when he monitored the pollen grains moving randomly suspended in water. The theoretical framework that could explain the experimentally observed phenomenon of diffusion was set up by Einstein in 1905. If there is no barrier in the medium the water molecules move according to Gaussian distribution. From the time of Robert Brown in 1810 when he recorded the oscillatory motion of pollen grains suspended in water, until the time Albert Einstein modelled kinetic-molecular theory in 1905, this random motion remained mystery. Einstein's theory states that each molecule is moved by thermodynamic effects, and follows a random path. Einstein modelled a relationship from microscopic scale to the macroscopic by introducing the diffusion coefficient D:

$$6\tau D = \left[x\left(t+\tau\right) - x\left(t\right)\right]^2 \tag{2.1}$$

where in one dimension, the water molecule is initially positioned at $x(t)$ at the time t and moves to the position $x(t+\tau)$ at the time $t+\tau$ due to diffusion. In the case of three dimensional displacement for many molecules, the relative displacement of a molecule at a position $\vec{x}$ is indicated by the vector $\vec{u}(\tau) = \vec{x}(t+\tau) - \vec{x}(t)$, which is a function of time τ. $\vec{u}$ is a displacement vector indicating both the magnitude and direction of Brownian motion. Therefore the diffusion coefficient is the dot product of the position vectors:

$$6\tau D = u\left(\tau\right) \cdot u\left(\tau\right) \tag{2.2}$$

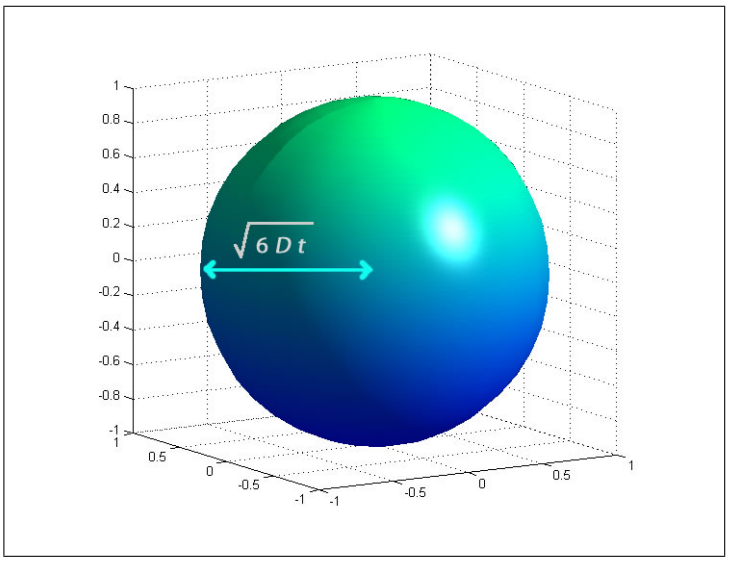

Figure 2.1 Gaussian diffusion in three dimension. The isoprobability surface is spheric with a radius of $\sqrt{6D\tau}$ centered at the origin.

Assuming that some water molecules are initially positioned at the origin and that they are followed in a time window of τ, then the molecules are expected to spread homogeneously around a circle of radius *l(τ)*. This characteristic parameter l equals to $l(\tau) = \sqrt{6D\tau}$ (Figure 2.1). It defines the intrinsic expansion of water molecules in a time period τ in case of isotropic diffusion. In biological tissues, the diffusion is not identical in all directions. The microstructure of the investigated tissue is aligned in one direction in fibrous tissues. Water moves more easily in the direction of this alignment than in the perpendicular direction [10]. Diffusion in such media differs from intrinsic diffusion, because it is dependent on the physical structure of the media. Therefore this kind of diffusion is called apparent or restricted diffusion. The name of Apparent Diffusion Coefficient *(ADC)* in the DTI literature comes from this fact. The diffusion tensor D where only one direction is promoted at each position is expressed as the tensor product of the displacement vectors:

$$6\tau D = u \otimes u^T \tag{2.3}$$

D is a tensor of rank two and is represented by a symetric 3×3 positive semi-definite matrix by its definition in Eq. 2.3. The tensor D in the generalized form of Einstein's relation is known as diffusion tensor. If anisotropic diffusion is in the media, Einstein's relation must be generalized to allow for directional dependence [11]. This matrix

represents a different shape rather then the spherical shaped expansion of isotropic diffusion, and it defines the ellipsoidal shaped expansion of the anistropic diffusion. The ellipsoid has three main axes which define the directions of the diffusion ellipsoid (Figure 2.3). These axes are determined by eigenvalue decomposition. The diagonalization of the D gives the in demand eigenvectors and eigenvalues e_1, e_2, e_3 and λ_1, λ_2 and λ_3 respectively (Figure 2.3). The first direction is the elongated part of the ellipsoid at a distance λ_1 of the origin and in the direction e_1, where e_1 is a unit vector. This dominant vector representing the largest displacement of the water molecules is named as the Principal Diffusivity Direction *(PDD)*. Regarding the eigenvalues the diffusivity is defined by $\lambda_1 > \lambda_2 > \lambda_3$.

This thesis focuses on the molecular diffusion of water in the human brain. The tissue of the human brain can be divided into three classes, white matter, grey matter and cerebrospinal fluid. In brain regions except white matter water, molecules can diffuse more or less freely in all directions, which results in isotropic diffusion (Figure 2.2). However, in white matter, restricted diffusion is observed (Figure 2.2). WM has longitudinally oriented structure, and its shape is defined through densely packed axons. The membranes of axon bundles are widely assumed to be the main barrier for water diffusion in tissue, hinder diffusion perpendicular to the fibers [12, 13]. In that case, the molecular diffusion is called anisotropic. The diffusion carries information about the underlying anatomical architecture of living tissues. This is exactly what diffusion imaging tries to study.

2.1.2 Diffusion in Magnetic Resonance Imaging Aspect

In 1956, H.C. Torrey mathematically showed how diffusion application changed the Bloch equations for magnetization [14]. Torrey modified the original Bloch's equation of transverse magnetization M_+, and included diffusion terms. Recalling that Bloch equations are equations of motion of nuclear magnetization, one can calculate the nuclear magnetization $M_+ = (M_x, M_y, M_z)$ in MRI as a function of time when relaxation times T_1 and T_2 are present. In a typical T_1-weighted image, water molecules

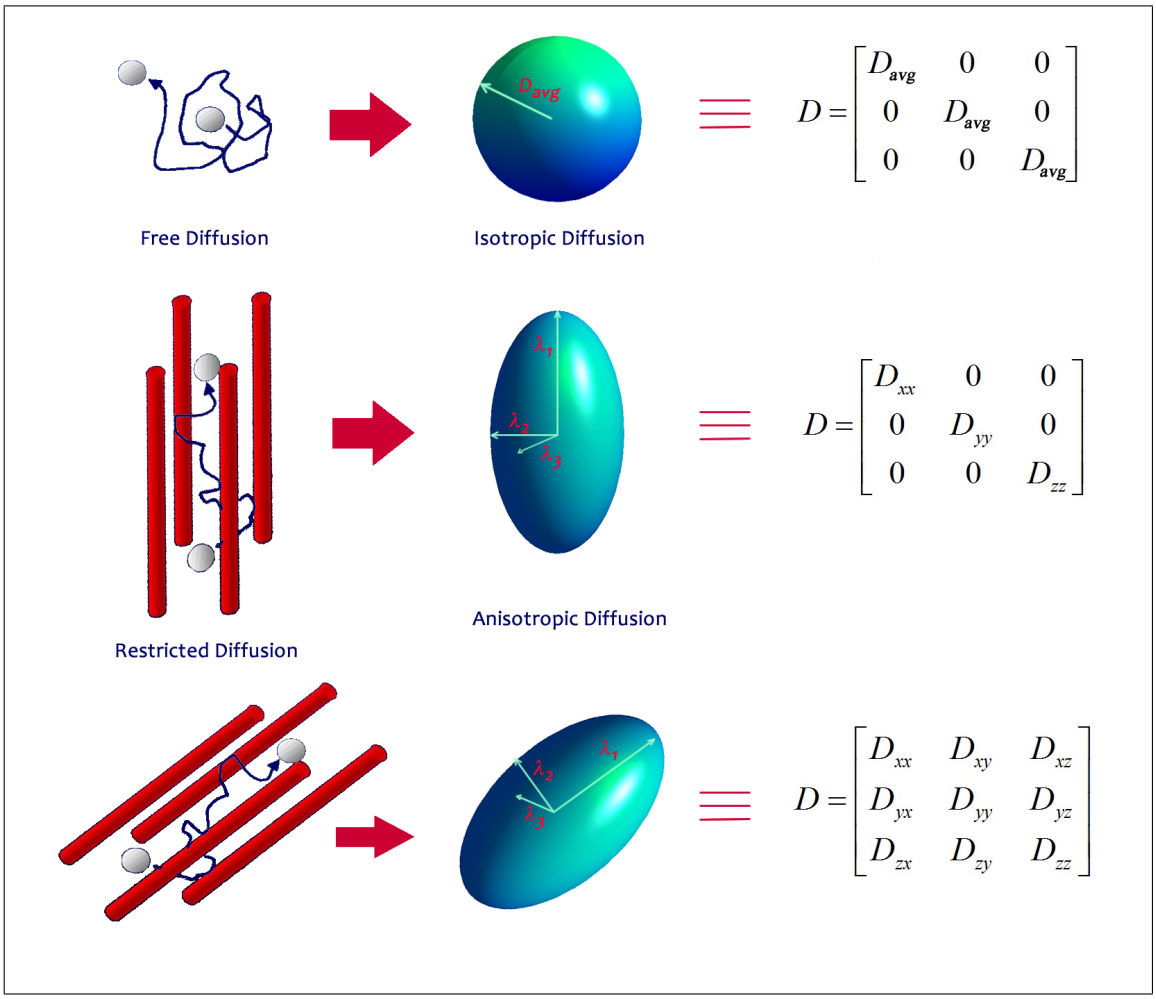

Figure 2.2 Relationship between anisotropic diffusion, diffusion ellipsoids, and diffusion tensor. The diffusion ellipsoid on the upper row shows unrestricted diffusion, or isotropic diffusion, where the diffusion is more or less equal in all directions: ($\lambda_1 = \lambda_2 = \lambda_3$). Diffusion can be characterized by diagonal elements (D_{xx}, D_{yy}, D_{zz}) all of which have the same *average* value D. The diffusion ellipsoid on the lower rows show a restriction of diffusion resulting from the surrounding tissue, in this case a myelin sheet, which restricts the movement of diffusion to directions parallel to the axons: ($\lambda_1 > \lambda_2 > \lambda_3$): Diffusion is mainly in the direction of the largest eigenvalue (i.e., prolateness). In anisotropic diffusion, the diffusion tensor is geometrically equivalent to an ellipsoid, with the three eigenvectors of the tensor matrix set as the minor and major axis of the ellipsoid.

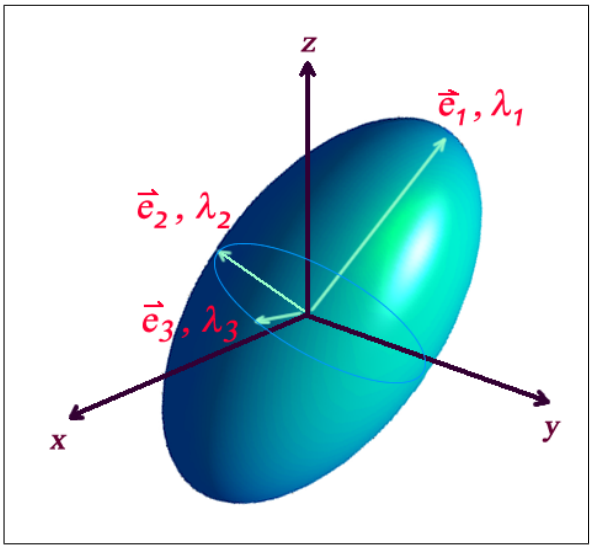

Figure 2.3 The diffusion tensor ellipsoid, the local tissue and physical gradient coordinate systems. The diagonalization of the positive definite and symmetric diffusion tensor results into three eigenvalues and three eigenvectors.

in a sample are excited with the imposition of a strong magnetic field. This causes a simultaneous precession of many of the protons in water molecules, producing signals in MR. In T_2-weighted images, the loss of coherence or synchrony between the water protons are measured and as result contrast is produced. In an environment, where water can freely move, the relaxation tends to take longer. In certain clinical situations, this fact is used to generate contrast between an area of pathology and the surrounding healthy tissue. MRI can be made sensitive to the Brownian motion of molecules. The ^{1}H atoms which are especially abundant in water, so in biological tissue too, have a nuclear spin angular momentum. These can be visualized as spinning charged spheres that give rise to a small magnetic moment. When a magnetic field $\vec{B}$ is applied to these spins, the magnetic moment vector tends to align along the direction of the field. The spins are seperated from the huge magnetic field $\vec{B_0}$ which varies between $1 - 11T$ via radiofrequency *(RF)* pulse $\vec{B_1}$. By that way, the spins are excited out of the equilibrium state, and become more aligned. The dephasing is achieved by applying a magnetic gradient $\vec{G}$ in the spatial direction during the reading process. Afterwards, the acquisition is performed. Finally, the spin signal coming from the component situated in the normal plane of $\vec{B_0}$ is acquired. The in terms of diffusion modified Bloch equation as

mentioned the Bloch-Torrey equation [14] is given by Eq. 2.4:

$$M_+(r,t) = M \times \gamma B - \frac{M^x e_1 + M^y e_2}{T_2} - \frac{M^z - M_0^z}{T_1} e_3 + \nabla \cdot (D \nabla M) \tag{2.4}$$

By varying the homogeneity linearly by a pulsed field gradient makes the MRI sensitive to diffusion. Torrey implemented the application of a spatially varying gradient to MR. Spin precession is proportionally dependent to the strength of the magnet. This causes the protons to precess at different rates. As a result, phase dispersion is generated and signal loss is achieved. A gradient pulse with opposite magnitude is used for rephasing the spins. Because of the signal loss, the refocusing will not be perfect. The pulse sequence resulting this reduced signal was initially invented by Stejskal and Tanner [15] 2.5:

$$S_i = S_0 e^{-b \hat{g}_i^T D \hat{g}_i} \tag{2.5}$$

where S_i is the signal received with the ith diffusion gradient pulse (for i equals 1 to N, (N=6 typically), S_0 is the signal received without the diffusion gradient pulse [16,17], b is the diffusion weighting factor, $|\hat{g}_i|$ is the strength of the ith diffusion gradient pulse, and $\hat{g}_i$ is ith diffusion gradient vector. The 3x3 diffusion tensor D is calculated from a set of diffusion weighted images for each pixel as in Eq. 2.5.

2.1.3 Pulsed Gradient Spin Echo Experiment

The pixel intensity in MRI is dominated by water concentration (proton density), whereas the signal relaxation times T_1 and T_2 also influence. In diffusion imaging pulsed magnetic field gradients are used to sense the signal intensity to the amount of water diffusion namely the diffusion constant defined in Eq. 2.5. The magnetic field B_0 points toward the magnet bore z axis, where the right-left orientation is x axis, and the up-down is y axis. The pulsed field gradient is generated by turning on the gradients for $1 - 100ms$ [18, 19]. The magnetic field $\vec{B_0}$ is homogenous, therefore water molecules have the same frequency until a field gradient is applied. Depending on their position the protons rotate slower with weaker $\vec{B_0}$ and faster with stronger $\vec{B_0}$

field, which causes a loss of the overall signal. After this dephasing period there is a time interval before the rephasing gradient. Dephasing and rephasing gradients have opposite polarity, identical strength and length. Therefore such a rephasing gradient causes the previously faster spins to resonate slowly in this rephasing period and the slower spins in dephasing move faster. This way the spins regain their phases. Applying identical opposite phase gradients causes the signal to be sensitive to molecular motions. This generates diffusion weighted signal. The explanation of this generation is that the perfect refocusing happens only when water molecules keep their locations while the pulsed field application [20]. The signal loss causes the imperfection where it enables the detection of diffusion motion. MR is not able to measure the phase of individual protons but it detects the failure in rephasing. It should be mentioned that the diffusion and the flow motions lead different outcomes. Flow or bulk motions (i.e. brain pulsation) of the subject are coherent motions, which result in perfect rephasing without signal loss and shift of signal phase. In principle, one can discriminate the incoherent motion and and the coherent motion, respectively the signal loss and the phase shift [20]. In practice, the flow might follow multiorientational path in a pixel. Small blood vessels are an example of this situation. Bulk motion is not rigid and uniform as in synthetic examples. So the coherent motion often leads to signal loss and interferes with the diffusion weighted signal [20].

Typical molecular displacement in a diffusion measurement is $1 - 20\mu$m [20]. A unipolar gradient pair and spin-echo sequence is mostly used for diffusion weighting. The gradient application will be discussed in the next chapter in detail. Both unipolar and bipolar gradient applications make the measurement sensitive to diffusion motion. Some parameters influence the signal loss. The time interval between the two gradients effect the signal loss. The longer it is, the more the signal is lost. The higher the diffusion constant D, the chance of the water molecules is greater to move in a fixed time interval [20]. The amount of initial dephasing calculated by multiplying the strength G and the length δ of gradients is another constraint in the signal loss. The resulting diffusion weighting can be changed vice versa by controlling the G, δ and Δ.

2.1.4 Diffusion Tensor Imaging

In previous sections, it's been highlighted that molecular diffusion is anisotropic in living tissue due to biological barriers, and that it tends to follow the path along the dominant direction rather than others. The anisotropic diffusion enables estimation of the underlying anatomical architecture of investigated living tissues.

Recently, DTI has emerged as a candidate method for the rapid, nondestructive reconstruction of brain anatomy. The principle of DTI relies in the signal attenuation caused by water diffusion in the presence of a magnetic field gradient (Eq. 2.5) [15,16]. The hypothesis tells that the rate of water diffusion is greatest in the direction of the fiber orientation, and therefore fiber direction may be determined by using DTI to estimate the primary eigenvector of the local diffusion tensor.

Diffusion Tensor Imaging has shown promise as a non-invasive tool for estimating the orientation and quantity of WM tracts in vivo. The process of using DTI data to estimate white matter structures is commonly known as tractography. DTI tractography is a unique imaging modality in that it offers the only clinically applicable means of non-invasively imaging the myelinated axonal structure of the human brain [2, 6, 21–24]. The accuracy of white matter anatomical maps obtained by DTI is more unclear due to the general inability of the diffusion tensor model to describe multiple orientational maxima within a single voxel.

If the diffusion is isotropic the water movement in all directions has the same amount building a spherical path. In such a case the diffusion is defined with only one constant namely the diffusion constant D. D is related with the diameter of the sphere. If water diffuses with varying amounts in different directions, then this is called anisotropic diffusion. Instead of a sphere in isotropic case, the movement of water molecules becomes oval shape in 2D and ellipsoid in 3D. This is called diffusion ellipsoid. In biological tissues mostly anisotropic diffusion happens. The anisotropic diffusion cannot be defined by a single diffusion measurement and by a single diffusion constant. The importance of the anisotropic diffusion is that it represents information about the

underlying anatomical architecture. In ordered structures such as axonal tracts, white matter fibers, the water molecules diffuse along these structures. This underlies behind diffusion tensor imaging. The determination of water molecules' pathways provides knowledge about the investigated tissue.

2.1.5 Mathematics of Diffusion Measurement

Vectors and tensors are independent of any particular coordinate frame, but they have a unique matrix representation in a given ordered basis. All bases in this work are orthonormal bases: the basis vectors are all unit length and mutually orthogonal. As a consequence, the otherwise important distinction between covariant and contravariant indices of the tensor may be ignored. Tensors that are represented only in orthonormal bases are called Cartesian tensors. This dissertation is only concerned with Cartesian tensors. A second-order tensor can be thought of as a linear transformation between vector spaces. A tensor D is symmetric if $D^t = D$. The orthonormality condition of a basis $B = [b_1, b_2, b_3]$ means that $b_i \cdot b_j$ results the Kronecker delta δ_{ij} as in Eq. 2.6. The Kronecker delta δ_{ij} is useful in transforming tensor expressions, where it helps for simplified expressions for components of vectors and tensors.

$$\delta_{ij} = \begin{cases} 1 \; if \; i = j \\ 0 \; if \; i \neq j \end{cases} \tag{2.6}$$

A vector v can be expressed in basis B as:

$$[v]_B = \begin{bmatrix} \upsilon_1 \\ \upsilon_2 \\ \upsilon_3 \end{bmatrix} \tag{2.7}$$

$$\upsilon_i = b_i \cdot v \tag{2.8}$$

$$[Dv]_B = [D]_B [v]_B \tag{2.9}$$

The matrix representation of tensor D in basis B is the matrix $[D]_B$ (2.9). Setting $v = b_i$ into this definition D is determined as in 2.10 and defined as in 2.11:

$$\begin{bmatrix} b_1 \cdot Dv \\ b_2 \cdot Dv \\ b_3 \cdot Dv \end{bmatrix} = [D]_B \begin{bmatrix} b_1 \cdot v \\ b_2 \cdot v \\ b_3 \cdot v \end{bmatrix} \tag{2.10}$$

$$D = \begin{bmatrix} D_{11} & D_{12} & D_{13} \\ D_{21} & D_{22} & D_{23} \\ D_{31} & D_{32} & D_{33} \end{bmatrix} \tag{2.11}$$

Six parameters are needed to uniquely define the anisotropic diffusion ellipsoid 2.3. These parameters define the lengths of the principle axes of the diffusion ellipsoid, and called eigenvalues λ_1, λ_2, λ_3. The orientations of the eigenvalues of the diffusion ellipsoid are the eigenvectors e_1, e_2, e_3. These six parameters to define the diffusion ellipsoid are measured at least by six measurements at noncollinear / independent directions. These parameters are calculated by using 3x3 tensor namely the diffusion tensor, and the imaging is the diffusion tensor imaging. The diffusion tensor calculation and analysis will be discussed in the next chapter in detail.

The diffusion anisotropy measurement along independent orientations resulting at least six diffusion constants to characterize the shape and orientation of the diffusion ellipsoid is the most popular way in diffusion tensor imaging (DTI) (Figure 2.7). A base image S_0 with $b = 0$ is used in the DT calculation (Figure 2.4 and Figure 2.5).

Figure 2.4 represents the Stejskal-Tanner formula labeled as Eq. 2.5 in Chapter 2.1.2. Practical application of the equation usually means taking its natural logarithm (Figure 2.4, Eq. 2.12). Diffusion constant D is extracted either directly from two experiments performed with and without the diffusion gradients or preferably by linear fitting of a series of signals acquired with different b-values. The Stejskal-Tanner for-

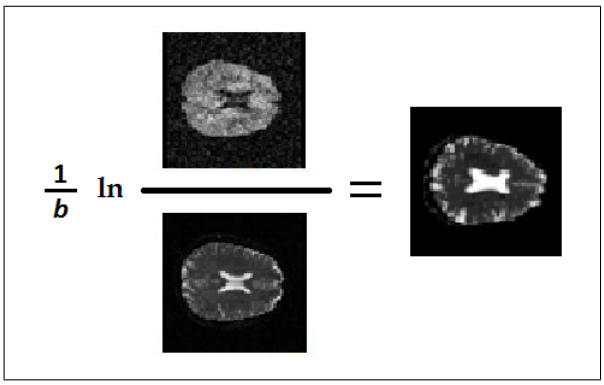

Figure 2.4 Calculation of the apparent diffusion coefficient Eq. 2.12: The natural logarithm of each exponential diffusion gradient applied image S_n is divided by the T_2 weighted image, and multiplied by the inverse of the diffusion weighting b.

mula can be derived using a very simple $1D$ diffusion model, it is valid more generally and correctly, and describes nuclear magnetic resonance (NMR) diffusion experiment in a homogeneous $3D$ environment as long as the diffusion behavior is Gaussian. Because this is not always the case, it is prudent to refer to the diffusion coefficient obtained from the Stejskal-Tanner formula as '*apparent diffusion coefficient*'.

In a 3D case, it is the diffusion gradient vector $G = (G_x, G_y, G_z)$ that determines the direction along which diffusion is measured. Diffusion perpendicular to the gradient vector does not alter the phase of magnetization in any way, therefore it is invisible. Essentially then, NMR experiments measure a $1D$ diffusion along the diffusion gradient vector. In an isotropic environment, application of a diffusion gradient along an arbitrary direction leads to the same signal attenuation predicted by the Stejskal-Tanner formula (Eq. 2.5). In an anisotropic environment, at least six independent $1D$ diffusion measurements are required to fully assess the six independent components of the diffusion tensor (Figure 2.2). Each of these measurements still obeys the Stejskal-Tanner formula except that the diffusion coefficient D must be replaced by a scalar quantity.

In DTI literature, the diffusion tensor (Figure 2.5) is commonly identified with the matrix representation in the coordinate frame determined by the MRI scanner

namely the laboratory frame, where the subscripts are x, y, and z as in Eq. 2.13:

$$\begin{bmatrix} x_1^2 & y_1^2 & z_1^2 & 2x_1y_1 & 2y_1z_1 & 2x_1z_1 \\ x_2^2 & y_2^2 & z_2^2 & 2x_2y_2 & 2y_2z_2 & 2x_2z_2 \\ & & \vdots & & & \\ x_n^2 & y_n^2 & z_n^2 & 2x_ny_n & 2y_nz_n & 2x_nz_n \end{bmatrix} \begin{bmatrix} D_{xx} \\ D_{yy} \\ D_{zz} \\ D_{yy} \\ D_{zz} \\ D_{xy} \\ D_{yz} \\ D_{xz} \end{bmatrix} = \begin{bmatrix} -\frac{1}{b} ln \frac{S_1}{S_0} \\ -\frac{1}{b} ln \frac{S_2}{S_0} \\ \vdots \\ -\frac{1}{b} ln \frac{S_n}{S_0} \end{bmatrix} \tag{2.12}$$

$$D = \begin{bmatrix} D_{xx} & D_{xy} & D_{xz} \\ D_{yx} & D_{yy} & D_{yz} \\ D_{zx} & D_{zy} & D_{zz} \end{bmatrix} \tag{2.13}$$

The calculation of distribution of signal phases by molecular motion is needed. The phase distribution in space is expressed as:

$$(x) = e^{iGx} \tag{2.14}$$

where x is the distance from the reference point (x=0), γ is the gyromagnetic ratio ($2.675x10^8 rad/s/T$ or $42.58 MHz/T$), G is the gradient pulse strength, and Δ is the duration of the pulsed gradient. The diffusion constant of water inside the brain is about $1.0x10^{-}3mm^2/s$ and the time interval namely the diffusion time is 30 ms. Einstein's equation defines the average diffusion distance in three dimension as in 2.15:

$$\sigma = \sqrt{6Dt} \tag{2.15}$$

The symmetric diffusion tensor has nine images representing the tensor elements (Eq. 2.13). The sample diffusion tensor elements are given in Figure 2.6 for a single slice in the data set. The off-diagonal images are mirrored on the diagonal images D_{xx}, D_{yy}, D_{zz}, which means there are only six different images corresponding to inde-

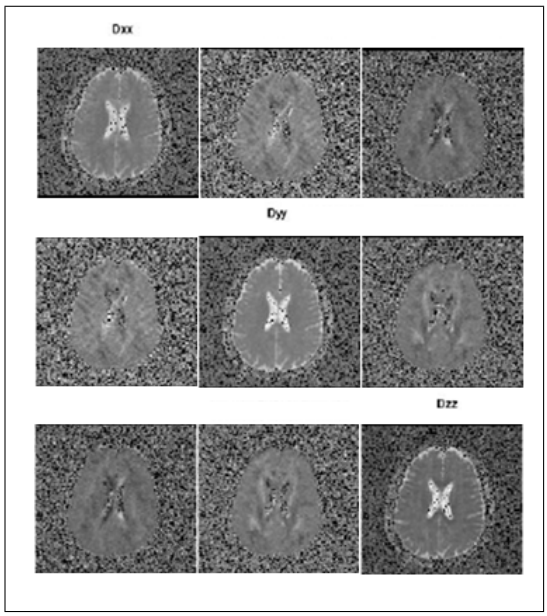

Figure 2.5 The symmetric diffusion tensor is presented with its actual tensor components arranged according to their position in the diffusion tensor in Eq. 2.13. Each of the nine images gives the tensor elements, of a single axial slice in the data set. The off-diagonal images are mirrored on the diagonal images D_{xx}, D_{yy}, D_{zz}, which means there are only six different images corresponding to independent tensor elements. The signal in the diagonal tensor elements is stronger and less noisy than in the off-diagonal images.

pendent tensor elements. The signal in the diagonal tensor elements is stronger and less noisy than in the off-diagonal images.

The approximate water movement is 8μm [20]. In the assumption of free diffusion, the water molecules motion is defined by Gaussian distribution [12, 20]:

$$1/\sigma\sqrt{2\pi} \cdot e^{\frac{-x^2}{2\sigma^2}} \tag{2.16}$$

The Gaussian distribution imply the population of water spins at location x. sigma defines the width of the distribution's curve, which means how far the molecules can move on average. Substituting the Einstein's equation in Eq. 2.16 following probability distribution is get:

$$P(x,t) = \frac{1}{\sqrt{4\pi Dt}} \cdot e^{\frac{-x^2}{4Dt}} \tag{2.17}$$

Here $P(x,t)$ gives the population of water at a location x at a time point t (where $t = \Delta$). The total signal S is the sum of the product of population and signal phase

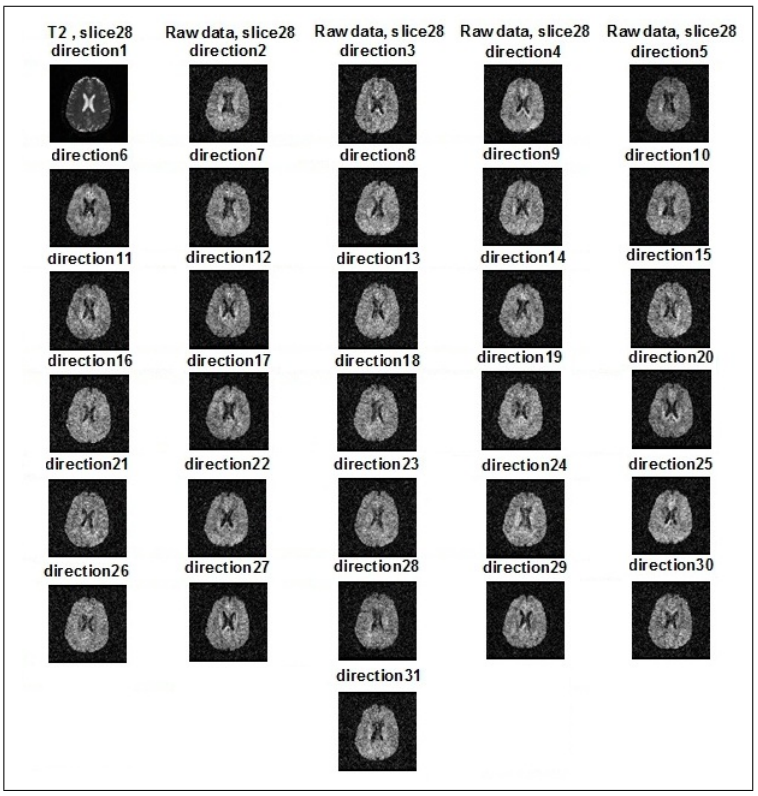

Figure 2.6 Example for diffusion weighted data for a single slice with 30 diffusion directions and a T2 image is presented. Diffusion weighted images are used to solve Eq. 2.12, and to calculate the diffusion tensor as in Eq. 2.13.

along location x [20]:

$$S = \sum_{x} P(x,t)\phi(x) \tag{2.18}$$

where $\phi(x)$ is the phase distribution in space (Eq. 2.19). It is introduced by a gradient pulse with a strength of G, a duration δ and the gyromagnetic ratio γ.

$$\phi(x) = e^{i\gamma G\delta x} \tag{2.19}$$

The amount of signal attenuation can be calculated by adding all the signal phases at each location (Eq. 2.20):

$$S = \int_x P(x,t)\phi(x)dx = \frac{1}{\sqrt{4\pi D\Delta}} \cdot \int_x e^{-x^2/4D\Delta} e^{i\gamma G\delta x} dx \tag{2.20}$$

If no gradient is applied, $G = 0$, this normalized signal phase (Eq. 2.19) becomes 1. So Eq. 2.20 becomes:

$$S = \int_x P(x,t)dx = \frac{1}{\sqrt{4\pi D\Delta}} \cdot \int_x e^{-x^2/4D\Delta} dx \tag{2.21}$$

The phase term is always less than 1. This generates a signal less than 1 in the presence of pulsed gradients ($G \neq 0$). In practice, there are number of signal intensities read from MR scanner [20]. Assigning the signal intensities with and without diffusion weighted gradients applied as S and S_0 respectively, the resulting signal equation corresponds to the well known Stejskal-Tanner equation, which leads to the calculation of the diffusion tensor D. The exponential decay can be rewritten in many forms, which gives the signal loss by diffusion weighting.

$$S = S_0 e^{-\gamma^2 G^2 \delta^2 D\Delta} \tag{2.22}$$

The diffusion constant can be calculated from the amount of signal loss, but not from the signal intensity.

2.1.6 Diffusion Tensor Tractography

The white matter architecture is reconstructed non-invasively by pixel-by-pixel fiber orientation knowledge revealed from DTI data. The computer-aided 3D fiber tract reconstruction techniques are called diffusion tensor tractography (DTT). The 3D tractography elucidates the anatomic brain structure and in some cases the pathology of the investigated brain tissue.

Tractography techniques rely in following the principle diffusivity of water cal-

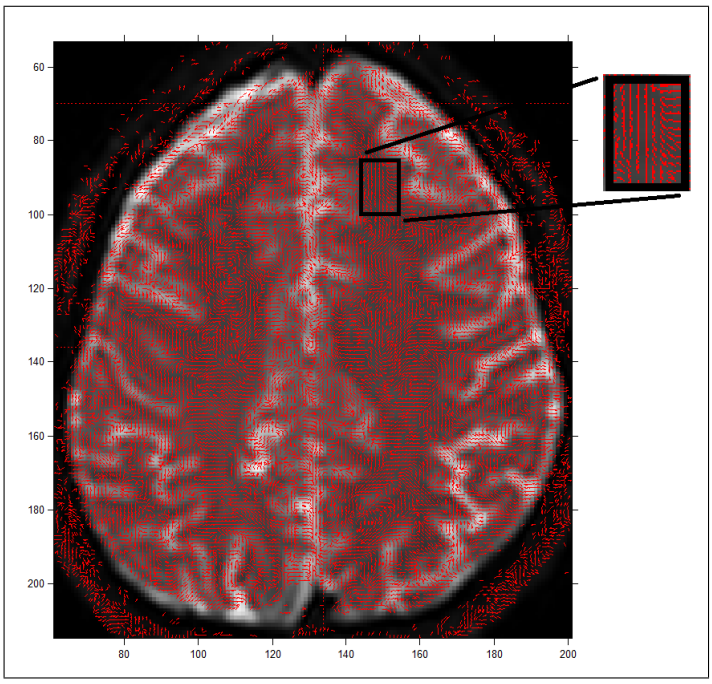

Figure 2.7 A representative cross section of the DTI's primary eigenvector direction which is overlaid on its corresponding intensity image.

culated from the diffusion tensor in each image voxel. Starting at a seed region, tractography provides the possibility to tract the white matter and its connectivity in living human brains. There are many prominent tracts in human brain that are large enough to detect visually. These major tracts can be clearly defined by DTI with 23 mm image resolution using the DTT.

The observation that the apparent diffusivity of water is greatest along the dominant orientation of white matter tracts within an image voxel has led to a variety of methods for displaying fiber orientation, ranging from simple techniques based on apparent diffusion coefficients measured in two orthogonal directions [25], to methods based on information contained within the full diffusion tensor [3, 26–28]. This orientational information has been further utilized in attempts to infer axonal connectivity in the brain [29–35]. In the majority of these methods, at each step in the reconstruction of a fiber trajectory a single estimate of fiber orientation is used to determine the direction of propagation. In tractography, accumulated uncertainties in fiber orientation have clear potential for leading to erroneous reconstructions of pathways. Some approaches have attempted to allow for the uncertainty in fiber orientation [33–37],

or have attempted to reduce the uncertainty in fiber orientation either through regularization approaches [32–35, 38] or through generating continuous approximations to the sampled tensor field and applying smoothing factors [36, 39]. Wittenbrink et al. [40] discussed this issue in some depth and described various glyphs for visualizing uncertainty in vector fields. Basser [41] later described an approach for constructing such a glyph or a "cone of uncertainty" in the estimate of eigenvectors obtained from DTI, i.e., a cone whose cone angle is equal to the uncertainty (i.e., a given confidence interval) in the estimate of the orientation of the principal eigenvector. However, this method was based on matrix perturbation analysis of synthetic data. No attempts to determine the uncertainty of estimates of fiber orientation in vivo from real data have yet been reported. The bootstrap method [42] is a nonparametric procedure that enables one to estimate the uncertainty of a given statistic, or its probability density function (PDF). Recently, Pajevic and Basser [43] proposed a nonparametric method for statistical analysis of DTI data based on the bootstrap method. This application of the bootstrap procedure has also been used by other groups to compare the performance of DTI acquisition schemes [44] and tractography algorithms [45] and is clearly a useful tool in terms of characterization of noise in DTI data.

The DTT literature can be covered on two general class of tractography approaches, i. deterministic and ii. probabilistic tractography. Tract reconstruction is based on tract propagation and energy minimization. Briefly, in the deterministic approach, a seed point is selected and a tractography results only one best-fit solution, where the probabilistic approach relies in defining the most probable connection path.

2.1.6.1 Deterministic Tractography. Tractography algorithms mostly rely on line propagation techniques to determine white matter tracts [46]. This first class of DTT is called deterministic streamline fiber tractography. Deterministic DTT algorithms mainly rely on seed based approach. The identification of a suitable seed (starting) region leads to initiate the algorithm. The next application step is the propagation of the track along the estimated fiber orientation. Finally, the termination of the tract is achieved when appropriate similarity criteria are met. Tractography

algorithms rely on the availability of estimates of the orientation of the white matter fibers at any location within the ROI. The principal diffusivity is typically assumed to provide a knowledge to estimate the fiber tract within each imaging voxel. The simplest method to obtain a deterministic tractography estimate is to use nearest-neighbor interpolation. The desired tract orientation is approximated as that of the nearest voxel [47]. The algorithm proceeds by stepping out from the seed position along the orientation estimated at that point, by a fixed user-specified step-size. As the orientation at the new pixel is determined, the algorithm follows along that direction until the tract is terminated. The fixed step-size tracking combined with nearest-neighbor interpolation is the idea of the original fiber assignment by continuous tracking (FACT) algorithm [29]. FACT algorithm is actually a first-order Euler integration procedure, and this is known as an approach that fails in highly curved regions due to the finite step size [48]. The implementations of deterministic tractography differ mainly in the choice of interpolation method. Other deterministic DTT methods have been proposed to allow fiber tractography to proceed through crossing fiber regions by "deflecting" the direction of tracking according to the diffusion tensor, rather than strictly following the principal diffusivity [49]. However, this deflection based approach has been shown an increase in the amount of overshoot in highly curved regions [50]. The applied arbitrary thresholds will force early termination of the reconstructed pathway. Here the arbitrary thresholds are anisotropy and angular thresholds. Mainly, there are two main reasons for the choice of similarity criterion. In low anisotropy regions, the major eigenvector of the diffusion tensor is poorly estimated and also noise sensitive. And as anisotropy tends to be high in white matter and low in gray matter, a sudden drop in anisotropy is assumed to be the gray/white matter boundary. And tracts are generally assumed to start and end at these boundaries. Angular threshold as another common criterion for termination, is based on the local curvature of the track. For DTT concerns, the angle between the directions of two subsequent steps should be in a certain predefined threshold. This constraint similar to the anisotropy threshold forces the propagation within the predefined similarity criteria, and the tract is not allowed to propagate any further like in the basic streamline tractography [1]. The motivation for angular threshold criterion is that a sudden change in direction of the local curvature of the tract is likely to be caused by artifacts in the data like noise. As a result of the

combination of these contraints, the stopping criteria in DTT include intersection with voxels characterized by low anisotropy values or large local curvature of the trajectory. These issues have limited the usefulness of deterministic approaches in defining certain fiber tracts especially in uncertainty regions where the anisotropy is low and the local curvature of the tract is crossing and curving.

2.1.6.2 Probabilistic Tractography. Noise is an important issue in the DTI. The noisy data introduces uncertainty in the estimation of fiber orientations. Consequently, the determined fiber tracts include errors [51, 52]. These errors might mislead the tractography and cause to detect completely different connections rather than the underlying white matter anatomy. Deterministic tractography algorithms provide a single unique estimate of the white matter tract from each supplied seed point, and a confidence interval is not considered around this estimate, which leads to a single best match estimate. Probabilistic algorithms, however, try to address this limitation, where their results are in the form of a probability distribution. Probabilistic algorithms have been proposed to characterize the uncertainty in fiber tract estimation. For each starting point, a set of possible trajectories is obtained for a given voxel. Here, each trajectory is generated in a streamline fashion. Therefore each propagation direction at each step which is being chosen at random from the distribution of directions available at the steps corresponding voxel, are guiding the algorithm to tractography [43–45].

Model-based probabilistic algorithms, model-free probabilistic approaches, bootstrap tractography and global optimization algorithms are different types of probabilistic DTT algorithms [53, 54]. In this study, the SOFMAT algorithm reconstructs the most probable paths in the brain space by unsupervised learning, such that path configurations are consistent with the underlying diffusion tensor knowledge and satisfy specified constraints. Compared with deterministic approaches, probabilistic approaches have the additional advantage in not restricting one tract per seed. SOFMAT approach allows the user to select various arbitrary brain regions at random as starting regions, and tries to estimate fiber tracts at each of these investigated regions. If the neighborhood function of SOFMAT and the predefined similarity constraints are

reached, the tractography results are identified. These results regarding to the selected starting regions, might be individual tracts or connections between these regions might be estimated. The the algorithm defines according to the applied criteria.

Probabilistic methods rely on the same underlying model as the deterministic methods, and many of them are based on deterministic techniques [48]. Most of the probabilistic methods are derivations or extensions of deterministic streamlines techniques. Therefore it should be emphasized that probabilistic tractography methods are not more accurate than the deterministic methods [48]. They also have the same limitations such as manual guidance and ROI-based editing. Probabilistic tractography's benefit is that results can provide an estimate of the precision with which a tract pathway has been reconstructed [48].

2.1.6.3 Limitations of Tractography. Tractography follows the principal diffusivity of the diffusion tensor. Typical resolution of the MRI signal in a voxel is limited, and this clearly reflects the significant difference between the scale of the axonal diameter and the imaging voxel size. Another limitation is the noise and artefacts in the diffusion data. DTT relies in the assumption, that the fibers visualised in each voxel are well described by a single orientation estimate. This assumption is not affective in uncertainty regions where there are more than one population of fibers with crossing, kissing or diverging. These pitfalls might lead to poor tracking of fiber tracts or even to determine fibers which do not exist. It should be emphasized, that the interpretation of tractography requires good neuroanatomy experience and a priori knowledge [4–6, 16, 48, 55]. There are several tractography algorithms represented in DTT literature. However, there isn't any gold standard which determines one as the most effective algorithm [48,55]. This gap is because of the lack of an objective way for assessment of the performances of the tractography algorithms against each other. This assesment also demands a knowledge of the precise anatomy of human brain tracts. Obviously this makes the problem very difficult.

2.1.7 Diffusion Tensor Analysis

The diffusion tensor D is a real, symmetric second order tensor, represented in matrix form as a real, symmetric, positive semi-definite $3x3$ matrix. Diagonalization of the diffusion tensor (Eq. 2.23) results in a set of three eigenvalues λ_1, λ_2, λ_3 listed in decreasing order. The eigensystem of the diffusion tensor may be interpreted graphically as an ellipsoidal surface with semi-major axis oriented in the e_1 direction and semi-minor axis oriented in the e_2 and e_3 directions [1]. The lengths of the axes in this ellipsoidal interpretation are given by the corresponding eigenvalues of each eigenvector, with semi-major axis length proportional to λ_1 and semi-minor axes lengths proportional to λ_2 and λ_3 [56]. In cases of purely isotropic diffusion, the diffusion ellipsoid takes a spherical shape, as $\lambda_1 = \lambda_2 = \lambda_3$. There are two extreme cases of physically realizable anisotropic diffusion [56]. For purely linear anisotropic diffusion, $\lambda_1 = \mathrm{c}$, and $\lambda_2 = \lambda_3 = 0$, the diffusion ellipsoid degenerates into a line pointing in the e_1 direction. In the case of purely planar anisotropic diffusion, the diffusion ellipsoid becomes oblate, meaning that $\lambda_1 = \lambda_2$, $\lambda_3 = 0$, and by means of the principal diffusivities, the diffusion is restricted to a plane spanned by e_1 and e_2.

2.1.7.1 Principal Component Analysis. Principal component analysis (PCA) is a classical statistical method widely used in data analysis and compression. PCA is based on the statistical representation of a random variable. The method reduces data dimensionality by performing a covariance analysis between factors. PCA method is based on linear transformations; however, nonlinear extensions exist. PCA is a technique for reducing second-order dependencies in the data by rotating the axes to correspond to orthogonal directions of maximum covariance (decorrelation). From a symmetric matrix such as the covariance matrix, an orthogonal basis by finding its eigenvalues and eigenvectors can be calculated. The diagonalization of the D results in three eigenvalues λ_1, λ_2, λ_3 (2.23). The eigenvectors e_i and the corresponding eigenvalues λ_i are the solutions of the equation (2.24), where the eigenvectors e_i are

the principal diffusion directions e_i $(i = 1, 2, 3)$.

$$D\,\vec{e_i} = \lambda_i\,\vec{e_i} \tag{2.23}$$

$$|D - I| = 0 \tag{2.24}$$

One way to solve the eigenvalue problem is to use a neural solution to the problem. The data is fed as the input, and the network converges to the wanted solution which is not applied in our present work. By ordering the eigenvectors in the order of descending eigenvalues, one can create an ordered orthogonal basis with the first eigenvector having the direction of largest variance of the data, which gives in our case the principal diffusivity. In this way, the most appropriate diffusivity directions can be determined. PCA is applied on the signal matrix to yield three uncorrelated (orthogonal) linear combinations λ_1, λ_2, λ_3 of the signal S_x, S_y, S_z. The first principal component λ_1 has maximum variance, and thus its weighting coefficients will give the direction of the maximum diffusion weighted signal, or largest principal diffusivity. The weighting coefficients of the second and third principal components λ_2 and λ_3 will give the directions of the intermediate and smallest principal diffusivity respectively.

The eigensystem calculation (2.23) for the analyzed image data provides information about the diffusion distribution throughout the investigated image. In diffusion tensor literature, tracking methods rely mainly on the dominant principal diffusivity λ_1, the dominant diffusion direction e_1. The assumption is that the fibers' orientation is along the principal diffusivity [29, 57–59]. An important element of diffusion tensor calculations is the sum of squares of the diffusivity differences (2.25). The square root of the sum of squares of eigenvalues is used to gain a weighted average, where the principal eigenvalue is the largest and therefore the dominant component. The result leads to well-known fractional anisotropy (FA) (Eq. 2.25) in diffusion tensor analysis. FA is used in DTI literature for thresholding the diffusion data (Figure 2.8). In our study, the FA map is used to minimize the input space. To compare the results, the algorithm is implemented without any FA selection where the whole input data was used in computation. The principle diffusion direction with thresholded FA map is

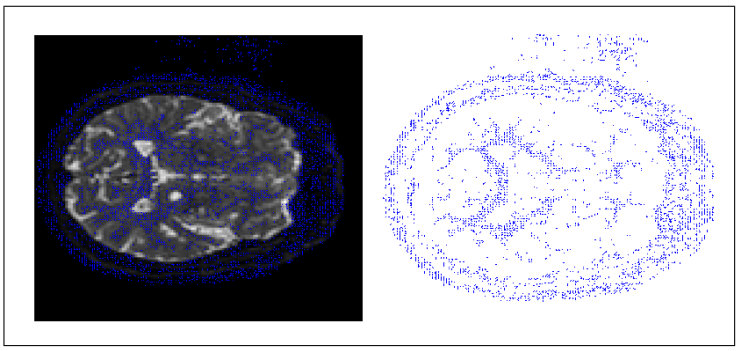

Figure 2.8 Left: Thresholded FA map superimposed on the T2 weighted image. Right: Thresholded FA map of the same image slice.

interpreted graphically in Figure 2.8.

$$FA = \sqrt{\frac{3}{2}} \frac{\sqrt{(\lambda_1 - \lambda_2)^2 + (\lambda_1 - \lambda_3)^2 + (\lambda_2 - \lambda_3)^2}}{\sqrt{\lambda_1 + \lambda_2 + \lambda_3}} \tag{2.25}$$

2.2 SOM: Self-Organizing Maps

The feature mapping model focused here described by Kohonen is arranged in a 1D lattice. In this topology, each neuron has a set of neighbors. The Kohonen model captures the essential features of computational maps in the brain and remains computationally tractable [7, 60]. Self-organizing maps are a special class of artificial neural networks based on competitive learning. Neurons are generating a lattice in one or two dimension. The neurons are selectively on while the competitive learning process according to the input pattern actually the stimuli. This process allows the winning neurons generate an ordered fashion with respect to each other for different input features [61]. The created meaningful coordinate system forms a topographic map of the input pattern. The coordinates of the input pattern are self organizing itself. In other words the coordinates of the neurons indicating intrinsic statistical features of the input pattern. A self organizing map can be seen as a nonlinear generalization of principal component analysis [7, 62].

2.3 PISTE: Artificial DTI Data

In an attempt to identify nerve fiber trajectories, several DTI based tractography techniques have been proposed to propagate diffusion tensor fields. Since it is difficult to validate the findings of a tractography method on brain images, artificially produced validated phantom images are used for benchmarking. One such commonly utilized dataset in DTI tractography method is called "Phantom Images for Simulating Tractography Errors" (PISTE). PISTE comprises a set of simulated fiber trajectories designed for testing, validating and comparing tractography algorithms allowing for the investigation of various geometries like linear, linear break, orthogonal crossing, and spiral [63]. Here, the linear trajectory is defined as a straight-forward linear tract, where the so called linear break trajectory of PISTE has a complete break at the tract [63]. As will be explained in detail in Section 4.1 , orthogonal crossing is an example of intersecting fiber structures. This PISTE trajectory is a crossing sample of two fibers intersecting each other at a right angle. Each of these trajectory sets contains a T_2 weighted image, an image with 6 elements of the diffusion tensor achieved by application of 30 different diffusion directions [31, 57], and an image of the corresponding eigensystem [63]. The tensor images of different geometries were fed into the proposed tractography system testing for varying SNR levels of 5, 15 and 30 as well as the noise-free condition. The PISTE images used in this study correspond to MR images acquired with $TE = 90$ ms, diffusion tract having a T2 of 65 ms, and the background with a T_2 of 95 ms. 30 diffusion directions were represented in 16 slices of 150 x 150 images. The diffusion directions are obtained using an algorithm analog to electrostatic repulsion [31, 57]. Although the eigenvectors of the dataset are given on PISTE site, a diffusion tensor analysis is also done, so the raw diffusion weighted images were also used to compute our own diffusion tensor images with the corresponding eigensystem. The analysis for every trajectory is done for varying SNR levels, such as 5, 15 and 30, and also noise-free. A detailed chart about the acquisition parameters is given in Table 2.1 [63].

The DT images are generated on the investigated trajectory with a decreasing anisotropy along the length of the tract, which is overlaid on a homogeneous anisotropic

background. The data used in this study is available as 32 bit float binary files at [63].

Table 2.1
Parameters of the simulated trajectories in PISTE.

Matrix Size	150 x 150 x 16
Diffusion Directions applied	30
b Value	1000 s/mm^2
Echo Time, TE	90 ms
T_2 of Background	95 ms

2.4 Visualization Tool

After implementation and evaluation of SOFMAT results on PISTE, the algorithm SOFMAT is implemented on real human data. The SOFMAT results representing the WM fiber tracts are visualized using TrackVis program version 0.5.2.2 [64,65]. TrackVis is a 3-dimensional visualization program that allows real-time visualization of the fiber track data that was created by SOFMAT.

3. Methodology

3.1 Novel DTT Methods

DTI is a fundamental technique that allows in vivo structural brain imaging by white matter estimation [1, 17, 26]. Differing from the weighted MR images, DTI provides directional information that could be used to compute nerve pathways [10, 39, 66]. The modality is unique in its ability to provide in vivo anatomical fiber tract information non-invasively [46]. However, the accurate estimation of white matter fibers is highly dependent on the tractography algorithm used. It is advantageous in clinical neuroscience, for quantitative comparison of specific white matter pathways in disease, in guided interventions, for the exploration of the normal brain anatomy. Tractography however, should be used with care because of the limitations of the technique [4, 5, 55]. A complete and validated neural fiber map of the brain is still not available in the literature, which makes the adequate verification of the post processing a challenging and a critical task.

3.2 Fiber Tracking: A Recursive Stack Algorithmic Approach

Here we propose a tool which aims to track the WM fibers according to stack data structure algorithm non-iteratively, depending on the structural information of the underlying tissue. Recursive stack algorithmic approach is proposed as a base to the developed SOFMAT. This approach allows to scan an ROI with respect of a predefined angular contraint, where the so called neighbor of the investigated node is checked whether it carries similar information with the starting node. The aim is to gain a proper linked list identifying the underlying structure. The stack is a data structure where data-item insertions and retrievals/deletions are made at one end, which is known as the top of the stack. Storing (inserting) a data item in a stack is called pushing it onto the stack, where removing (retrieving/deleting) a value from

a stack is called popping the stack. A stack behaves like a linked list in which all insertions and deletions are performed at the list head. The last node in the list is called "top", where the first node is called "bottom". Because the last inserted data item is the first retrieved/deleted data item, developers commonly refer to stacks as LIFO (last-in, first-out) data structures [67]. As seen in Figure 3.1, the stack builds down in memory. For each data-item push, the previous top data item and all lower data items move farther down. When the time arrives to pop a data item from the stack, the top data item (which in the flowchart in Figure 3.1 and Figure 3.3 reveals as "[3,2]") is retrieved and deleted from the stack.

The linear data structure used here helps to create a list of investigated region of interest of eigenvectors. The input eigenvectors serve as data-item, and the insertions and retrievals/deletions made at the top of the list leads to estimate the tract. The created list can be called a linked list in which all insertions and deletions are performed at the list head (top) [67]. For each data-item push, which means adding another eigenvector from the input space into the search, the previous top data item and all lower data items move farther down. When an eigenvector does not fit the similarity measure, which is an angular deviation allowance here, then the time arrives to pop this data item from the list, and the top data item is retrieved and deleted from the list. To clarify the implementation routine, application steps are summarized in a flowchart in Figure 3.1 and explained on the synthetic data as shown in Figure 3.2.

The starting point is selected as x=1 and y=1 as shown in Figure 3.2 as (1,1). This selected coordinate having the eigenvector [1,0] is the bottom of the stack.

The stack is a data structure where data-item insertions and retrievals/deletions are made at one end, which is known as the top of the stack. Storing (inserting) a data item in a stack is called pushing it onto the stack, where removing (retrieving/deleting) a value from a stack is called popping the stack. Now the implementation routine can be interpreted as follows:

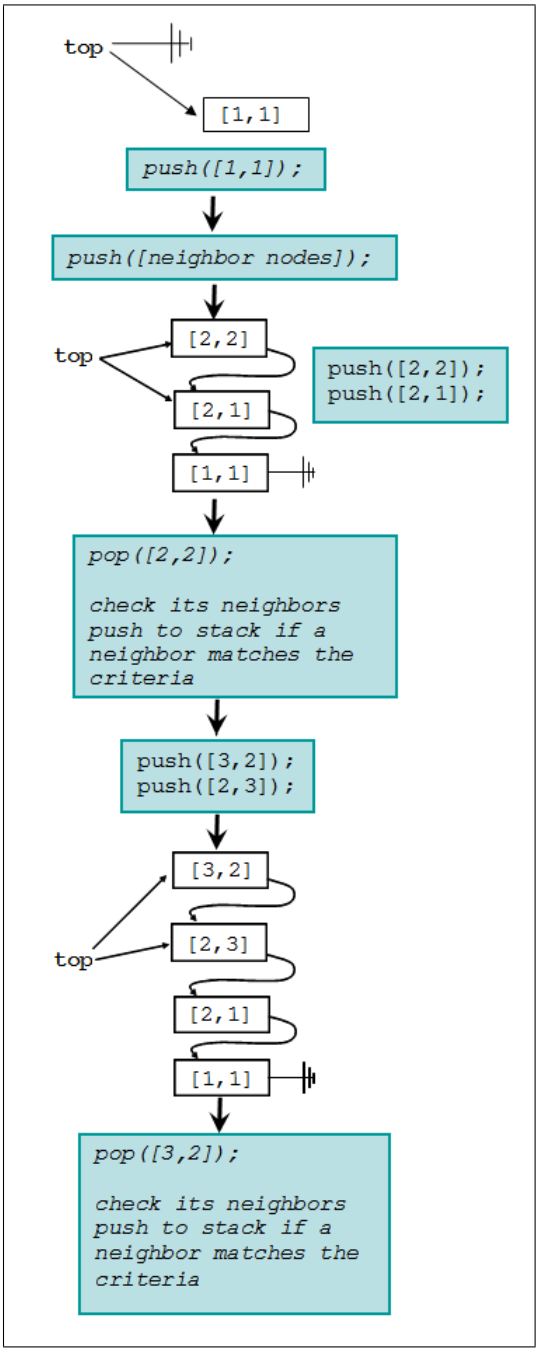

Figure 3.1 Flowchart of the stack linked list application.

1. Coordinate (1,1) having the eigenvector [1,0] stored in the stack as a starting point.
2. Pixel (1,2) is not within the limits of similarity measure.
3. Pixel (2,1) is stored in the stack on the top again in compliance with similarity. Top is now assigned to the new node.
4. Next, pixel (2,2) fulfilling the similarity measure is stored on the top the stack.
5. Pop pixel (2,2). Compare its eigenvector [0.7 .07] with its neighboring pixels' eigenvectors for similarity.
6. Eliminated neighbors: (1,3) and (3,3) with both having the eigenvector [-0.7 -0.7].
7. Push (2,3) and (3,2).
8. Pop pixel (3,2). Check its neighbors.
9. Pixels (2,3), (2,1), (2,2) satisfy the predefined similarity rule. But they are already in the stack, and they are already in the track matrix. Therefore these points are not pushed into the stack.
10. Neighbor pixels (3,1), (4,1), (4,2), (3,3) of (3,2) are not fulfiling the similarity criteria.
11. Pixel (4,3) satisfies the criteria. It is pushed on the top of the stack.
12. Similarly the next pixel to be pushed into the stack is (4,4).
13. As the search reaches to the boundary of the ROI with no further need for push search process of the network in the selected limits is completed.

The implementation results a stack which behaves like a linked list. Our approach relies in the assumption that the axon follows a unique path. Each element in the stack linked list implementation represents a voxel in the ROI, and each voxel is related with its neighboring voxels. The implementation steps of the list stack (Figure 3.2 and Figure 3.3) are as follows:

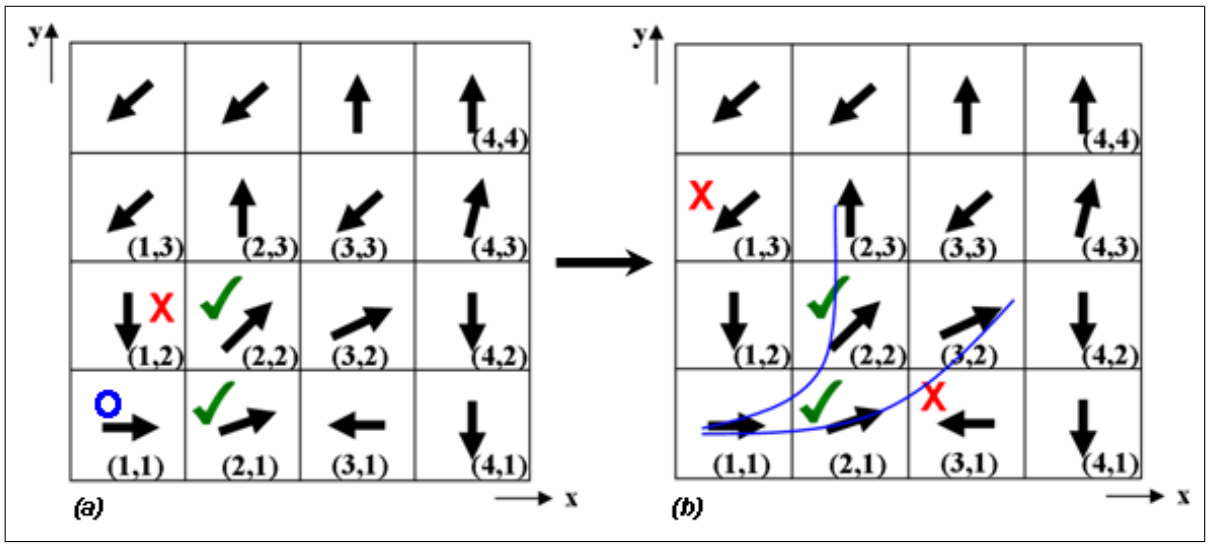

Figure 3.2 Sample synthetic eigenvector pattern. (a) $(1,1)$ is the starting node, where green checks represent the neighbors within the similarity measure.

The starting point is selected as $x = 1$ and $y = 1$ as shown in Figure 3.2a. This selected coordinate having the eigenvector $[1, 0]$ is the bottom of the linked list. The predefined similarity measure is a set of angular thresholds $\pi/j(j = 4, 6, 12, 18, 20)$. Pixel $(1, 2)$ is not within the limits of similarity measure $\pi/4$ (Figure 3.2 a). Pixel $(2, 1)$ is stored in the stack on the top again in compliance with similarity. Top is now assigned to the new node. Next, pixel $(2, 2)$ fulfilling the selected similarity measure is stored on the top of the list. The eigenvector $[0.7, 0.7]$ with its neighboring pixels' eigenvectors are being compared for similarity. As a result, neighbors with coordinates (1,3) and (3,3) with both having the eigenvector $[-0.7 - 0.7]$ are eliminated (as seen in Figure 3.2 b). The implementation follows by pushing the coordinates (2,3) and (3,2) to the list. Pixel (3,2) is popped. Then its neighbors are examined as in Figure 3.3 a. The routine follows by determining pixels matching with the predefined similarity rule $\pi/4$. The synthetic fiber path (represented in blue) is defined as a result as in 3.3 b.

Selecting the similarity measure as $\pi/4$, allows the pixel (2,2) to be on the list as described above. But examining the pattern by a different iteration for a varying angular threshold such as $\pi/6$ or $\pi/12$, this pixel is not being assigned for the neighboring pixel list. As a result the track represented in red on Figure 3.3b is the outcome of the computational routine. The decision making here about to select a track follows regarding to the underlying tissue's structural information.

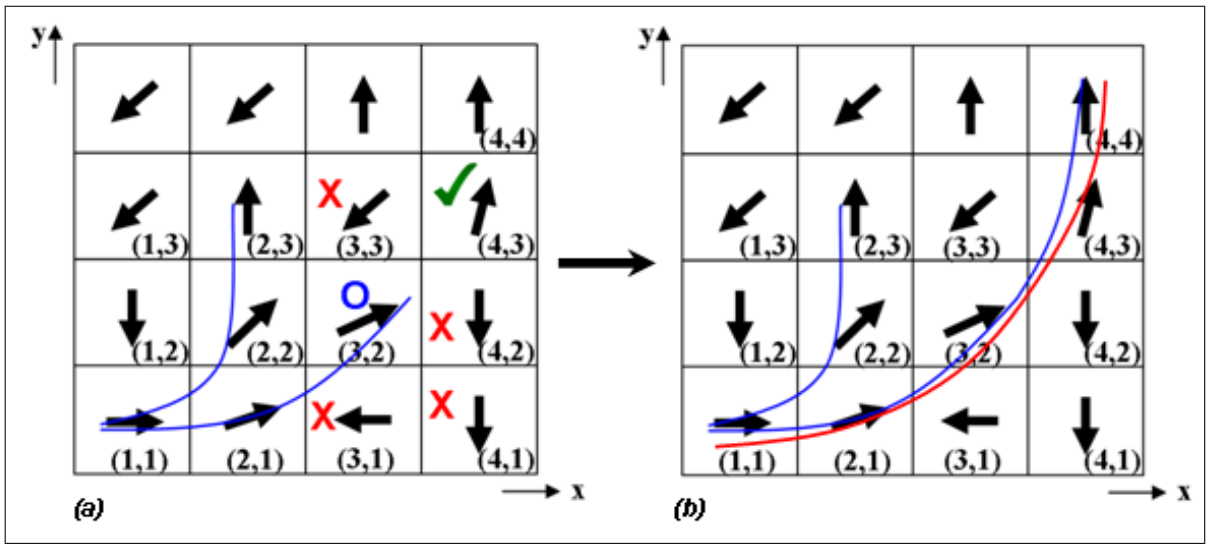

Figure 3.3 Listed data structure analysis results shown on sample pattern with its principal eigenvectors. Two possible resulting fiber paths are represented.

Tracking process is completed by popping the stack one by one each time searching for similarity of unattended pixels. Pop operation continues until stack is cleared based on LIFO. Read out results are displayed as fiber tracking paths.

The application follows with the investigation of the neighbors of the examined node within one pixel neighborhood. If one neighbor of the bottom point has an eigenvector in the predefined similarity measure then this point will be pushed/added to the stack. If one investigation node with the proper limits, added into the stack is being encountered several times, than no action is taken in case of the repetitions, because this node has already been pushed into the stack. When a pixel is pushed into the stack, its eigenvector is kept in track matrix even if the pixel is popped later in the process. The similarity measure resulted in a push action for a pixel in the neighborhood of the top of the stack is defined as an angular difference. We tried a number of angular thresholds for similarity, such as $\pi/4$, $\pi/12$, $\pi/20$.

The proposed approach relies in the assumption of the unique path description of an axon. Each element in the implementation represents a voxel in the ROI, and each voxel is related with its neighboring voxels. Regarding the neighboring voxel knowledge, the computation sorts the elements in the list for tracking, where the elements which do not fulfill the criteria are kept in a secondary matrix. While examining

the investigated pattern pixelwise, the elements in the secondary matrix come up as potential neighboring pixels in question. The repeated check for if they are within the similarity criteria and if they belong to the fiber track gives the chance of a double check in the system. By that way, the neighboring is updated and a more secure resulting track is being defined and followed. The routine updates itself so that for the one selected starting node the first and second neighboring pixels are investigated and the computational routine is stretched to a wide range via this increased neighborhood.

3.2.1 Results

The proposed method is implemented on simulated fiber eigensystem to determine the predefined synthetic trajectories (Figure 3.3). The output of the algorithm is in agreement with the visual inspection results as shown in Figure 3.4. Variation of the similarity measure causes major differences in the calculated neural path. Small values of the similarity measure decreases the number of voxels in the solution which are defined by the decision making as neighboring voxels while increased similarity measure selections generate more well defined and close results to the underlying tissue structure. Following the promising results of the synthetic data implementations, the method is applied on real DT brain images. As explained in detail in Section 2.1 (Eq. 2.23 and 2.24), the eigensystem of D is determined by PCA, and interpreted graphically as seen in Figure 3.4.

3.3 Self Organizing Nerve Fiber Tractography in DTI

Adequate verification of the post processing of DT analysis is challenging and critical task. An important drawback in the determination of the fiber paths for tractography purposes occurs in uncertainty regions where at least two fiber paths intersect. This study proposes an artificial neural network approach named SOFMAT based on Self-Organizing Feature Mapping (SOFM or SOM) to define the fiber tracts based on their diffusivity and to clarify, especially the fiber tracts in these uncertainty regions.

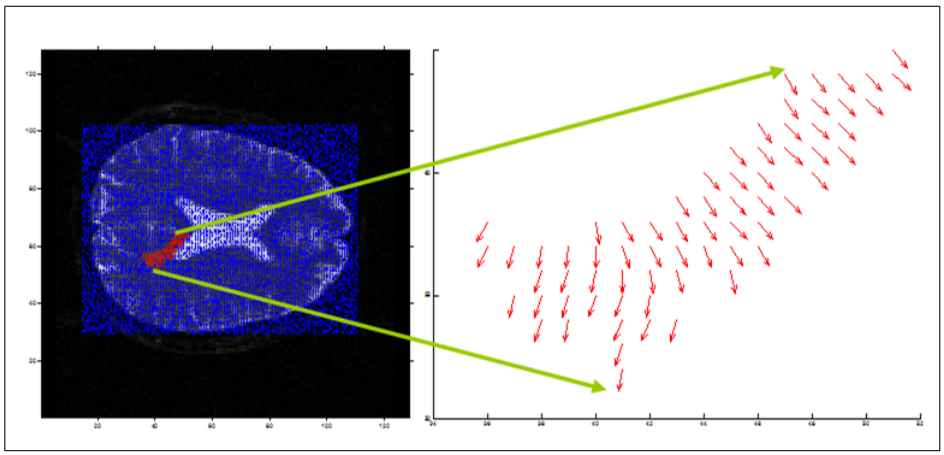

Figure 3.4 Fiber tracking results traced on axial slice with a similarity measure of $\pi/20$. Calculated neighboring pixels (red) with related diffusivity mapped on entire eigenvector map.

The locally computed diffusion tensors shape the randomly distributed artificial neuronal topology. The developed novel SOM based tractography approach SOFMAT (Self Organizing Feature Mapping Tractography) is based on unsupervised learning method, which is used in the training of Artificial Neural Networks (ANNs). Unsupervised learning is preferred for the fact that we do not have a reliable training set either for the pathological or for the normal human brain. SOM as a classifier demonstrated successful identification of structured topologies in various domains [7,60]. Representing a sub-set of ANNs, SOM is particularly useful in investigating multi dimensional topologies. In this study, the topology sought is actually the tracts of localized diffusion eigenvectors, which define the principal diffusivity of the fibers in the DTMR images. The available anatomical atlases depicting nerve tracts have poor resolution capable of distinguishing millions of axons contained in unit imaging voxel. Clinical validation data is hard to come by for the intended clinical utilization. Instead, it is a common practice to employ artificially produced data to evaluate proposed tractography algorithms. Therefore, in this study, a common diffusion tensor resource named PISTE (Phantom Images for Simulating Tractography Errors) is used for benchmarking the accuracy and acceptability of the proposed approach. The idea of SOFMAT is to accomplish the fiber pathways by considering each individual voxel's contribution taking into account the neighboring voxels' behavior in the topology. This is achieved by both competing and cooperating behavior of SOM nodes (neurons) in forming the topology. The proposed method has been tested on four Phantom Images from PISTE

with various signal to noise (SNR) values. The images represent various levels of complexities involving, cross-overs, kisses, direction changes. The results were than compared against well accepted tractography algorithms reported in the literature (i.e. Streamline (STL) [1] method and Guided Tensor Restore Anatomical Connectivity Tractography (GTRACT) algorithm [47]. Preliminary studies indicate that SOFMAT method gives promising and relatively superior results compared to the traditionally implemented and well-accepted tractography algorithms mentioned above.

This section of the thesis is organized as follows: In the next Section, a brief background work related to the proposed method is introduced including the synthetic data resource utilized for evaluation. Section 3 describes the method of the presented work in detail addressing how SOM is implemented to detect nerve tracts, and how the results have been validated. The related Results Section presents quantitative comparison of the proposed method against the commonly used algorithms. The discussions are given in the last Section.

3.4 SOFMAT: Self-Organizing Feature Mapping Tractography

SOFMAT (Self-Organizing Feature Mapping Tractography) is proposed as a tractography algorithm in this study. It is based on Self Organizing feature Maps (SOMs), a family in artificial neural networks. The advantage of SOM lies in its ability of mapping high dimensional data into a 1D, 2D, or 3D data space, subject to a topological ordering constraint [7, 60]. SOM is able to learn an input pattern in terms of the patterns' regularities and correlations. As will be explained in Section 3.4, the network adapts the output pattern according to its input. One important feature of SOM is that it is able to process noisy data. This makes the learning rule applicable in diffusion tensor fiber tract analysis. Based on this special class of ANN, the proposed algorithm SOFMAT aims to map the brain's diffusion tensor data into fiber tract paths using an unsupervised learning method. Unsupervised nature of the learning is essential, since the ultimate challenge is to identify the tractography of brain nerve pathways with no apriori anatomical or pathological information.

SOM orders the data into meaningful topologies corresponding to the given input data. SOFMAT uses this ability in terms of retaining the underlying structure of the input space and enabling a mapped match of the investigated imaging space resulting in nerve fiber tracts as an output. The final tractography is the converged state of an artificial neuronal map obtained by the iterative synaptic weight update process [7,60].

SOFMAT, in an attempt to discover nerve fiber tracts utilizes an artificial neural network learning scheme inspired by the self organization in a neurobiological system [6]. This is achieved by implementing the characteristics and basics of SOM unsupervised learning methodology onto the DT eigensystem. Here, each neuron's spatial location in the resulting feature map corresponds to a particular topology of the input data. Differing from a classical SOM application, SOFMAT utilizes the orientation information (λ_1, λ_2, λ_3, e_1, e_2, e_3) inherent in the DT images, along with the positional dependency. In other words, SOFMAT enables the analysis of correlated neighboring nodes with respect to both their spatial locations, and the direction of their diffusivities. The "diffusivity informed" SOFMAT uses this information as a topological ordering constraint.

The feature mapping model which SOFMAT implements in this study is arranged in a number of 1D lattices, as described by Kohonen [60]. In this topology, each neuron has a set of neighbors which are influenced by the motion of a target neuron defined by a weighted Gaussian distance function, as explained in detail in Section 3.3. The lattices formed as a result can take any arbitrary shape in the n-dimensional input space, even though they are nothing more than strings, as is also the case for axons forming a nerve tract. The proposed method benefits from this feature in detecting the topological nerve fiber map.

3.4.1 Competitive process in SOFMAT

SOFMAT inherits unsupervised competitive learning from SOM with the following principles [7,60]:

- The output neurons of the network compete among themselves to be fired, for a given input pattern.

- Only one output neuron is activated at any one time, called the winning neuron.

- The winning output node is processed by the self-organization progressing towards the input pattern I, while dragging its neighbors.

- As an outcome of this self-organized competition and cooperation the topological connectivity in I is maintained and reflected in the output.

- The input pattern I selected randomly is represented as in Eq. 3.1:

$$I = [x, y, z, \lambda_1, \lambda_2, \lambda_3]^T \tag{3.1}$$

where x, y, and z correspond to the three position coordinates, and λ_1, λ_2, λ_3 are the three eigenvectors of the diffusion tensors computed for the related diffusion tensor images.

- The input space pattern I and an output node similarity, or distance is determined in relation to the associated synaptic weight vector of each output neuron (node) expressed as [7] in Eq. 3.2. Here similarity match is reached by identifying the node that best matches the input I, and this winning neuron *P(I)* is found at a time step t by using the minimum-distance Euclidean criterion [7], where n is the total number of neurons in the network. As the network learns the mappings desired, weights are adjusted among the inputs to minimize error.

$$P\left(I\right) = argmin_j \left\| I\left(t - w_j\right)\right\|, j = 1, 2, \ldots, n \tag{3.2}$$

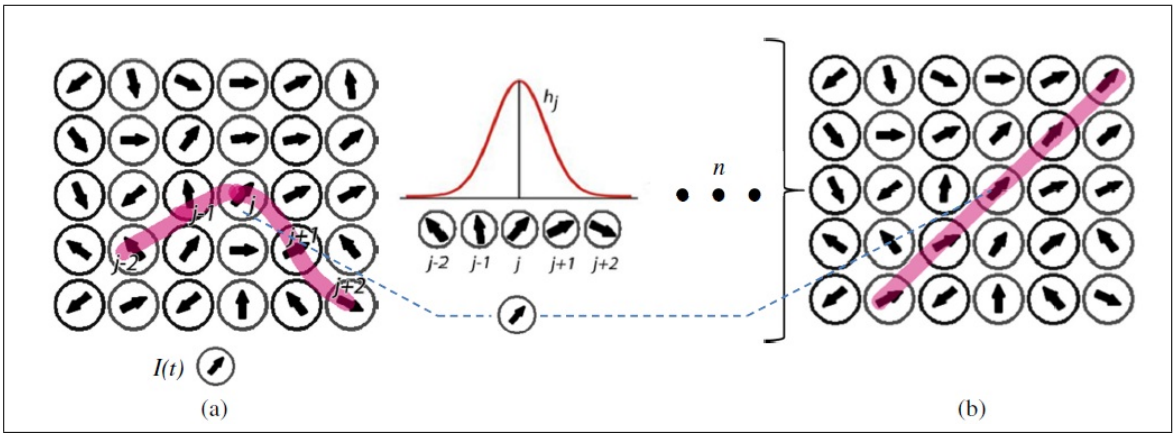

Figure 3.5 Illustration of the training process. (a) Initial random state of the lattice. The input data vector is displayed here as *I(t)*. Randomly initialized network after a learning step; intermediate stage of self-organization. Best match is assigned as winning node. Updating the weight allows the network to find its best matching nodes in the discrete output space (3.2). The nodes within the neighborhood h_j learn from the winning node. (b) Fully trained network after n iterations: Structured input space.

where w_j is the weight vector for the jth node as:

$$\vec{w}_j = [w_{j1}, w_{j2}, \ldots, w_{jm}]^T \tag{3.3}$$

In SOFMAT, m is defined as 6 corresponding to the number of diffusion gradient pulses (2.5). The first three elements of w_j describe the position of jth node, and the last three correspond to the orientation of the vector connecting the jth node to the j+*1*st node.

SOFMAT identifies the winning neuron by computing a distance function comparing an input pattern I with the synaptic weight vectors, w_j for each node (3.2). The training process is illustrated in Figure 3.5. First, the weight vectors are mapped randomly onto a two-dimensional lattice. Figure 3.5a represents this initial random state of the lattice. Training of the network gives the closest match to the input data vector *I(t)* in the node (Figure 3.5b). The nodes within the neighborhood h learn from the winning node (Figure 3.5c). The weight vectors within the neighborhood h learn from the input data vector and get updated. In Figure 3.5d, the final, fully trained network is displayed.

3.4.2 Cooperative process in SOFMAT

Cooperation in SOM algorithm is also inherited in SOFMAT. The level of cooperation of the neighborhood neurons is decided by the winning neuron (Eq. 3.2).

- The topological neighborhood h_{ji} (Eq. 3.4) is typically chosen as a Gaussian function [4]:

$$h_{j,i(x)(t)} = e^{\left(\frac{d_{j,i}^2}{2\sigma^2(t)}\right)} \tag{3.4}$$

$$\sigma\left(t\right) = \sigma_0 e^{\left(\frac{-t}{\tau_1}\right)} \tag{3.5}$$

where r is the sequential distance and d_{ij} is the Euclidean distance between the winning neuron *P(I)* and the other neurons *(j)* in the string, and calculated by the sequential distance r of I and j as given in Eq. 3.6:

$$d_{j,i}^2 = \left\|r\left(j\right) - r\left(I\right)\right\|^2 \tag{3.6}$$

The width, $\sigma(n)$, of the Gaussian neighborhood function decreases for facilitating convergence at an exponential rate, and the neighborhood shrinks in each iteration. The dependence of σ in discrete time t (t=0,1,2,) in Eq. 3.5, contributes to the convergence of SOM learning algorithm by excluding more nodes from the neighborhood iteratively. σ_0 is the initial value of σ, and τ_1 is the time constant, which are determined by ad-hoc methods influenced by the size of the input space and the number of output nodes as described in [60].

3.4.3 Adaptive process in SOFMAT

For a given input pattern I, all the neurons in the vicinity of the winning neuron *P(I)* are updated by a distance coefficient decreasing with the neighboring function, hj, i. It should be noticed, that hj, i is 1 for the winning neuron, and decreases ex-

ponentially as the nodes gets away from the winning neuron. The iterative learning process is actually representing the adaptation of the weight vectors towards an input pattern I and given as (Eq. 3.7):

$$\vec{w}_j(t+1) = \vec{w}_j(t) + \eta(t)\, h_{j,i(I)}(t)\,(I - \vec{w}_j(t)) \tag{3.7}$$

Eq. 3.7 gives the computation of the updated weight vector $w_j(t+1)$ at time *t+1*, with a time varying learning rate $\eta(t)$, where $w_j(t)$ is the synaptic weight vector of neuron j at time t [7, 60]. As introduced in Eq. 3.1, our input space I consists of the positional elements x, y, and z, and directional elements λ_1, λ_2, λ_3 for each voxel. The SOFMAT is shaped by comparing each input vector I, to every node, in the neighborhood (Figure 3.5). The comparison is based on both position and orientation according to Eq. 3.2. Once the winning neuron is determined, the positions of the nodes are updated according to Eq. 3.7. The directional vectors of the SOFMAT nodes are updated according to the newly formed neuronal topology as in Figure 3.6. Assuming that nerve tracts are formed from multiple axons, we provided multiple strings with an expectation to detect the underlying neuronal pathways. Multiple strings implementation methodology is summarized as follows:

SOFMAT with multiple strings:

- Initially there are N_y strings each of which is made of N_x nodes.
- Initial position and orientation of each node w are randomly initialized.
- For each node of the input pattern, I,the winning neuron is computed based on the minimization of the cost function as given in Eq. 3.2. The winning node also determines the winning string.
- Once the winning neuron and its string are determined,

  a) a weight update matrix $w_j(t)$ is computed for that string using the position information according to Eq. 3.4, 3.5 and 3.7.

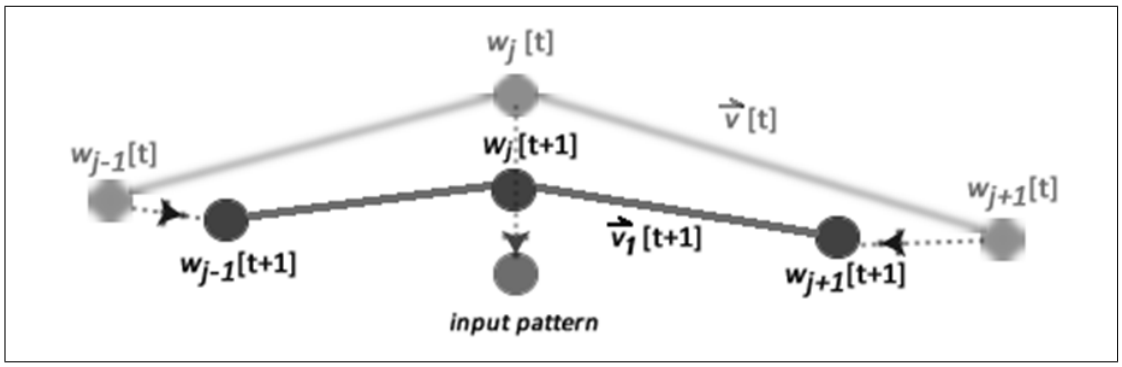

Figure 3.6 The pixel with the weight w_j at time t, nearest to the input pixel is winning, and is moving towards this input pixelaccording to Eq. 3.7 as shown with an arrow in the Figure. Its neighbors w_{j-1} and w_{j+1} at time t on the string are also moving to a lesser extent. The update in the orientation can be recognized through initial weight vector *v[t]* and updated resulting vector *v[t+1]*. Units close to the winner as well as the winner itself, have their weights updated significantly. Weights associated with far away output pixels do not change significantly. The update continues until the sought topology is found and the feature map is consistent.

b) the weight update matrix is computed for that string for updating the orientation information according to the new position as in Figure 3.6.

- This procedure is repeated from step iii until the maximum number of predefined iteration or convergence is reached.

- The converging weight matrix that includes the position and orientation information of the multiple strings is the resulting topology of SOFMAT.

The aim of the implementation is to map the underlying topology of a discrete input space. Initially, the weights are assigned randomly and the SOM pattern is arbitrarily positioned. A starting input node is randomly picked among the inputs for training (Figure 3.6). The node with the closest reference vector represents the winning neuron $w_j(t)$. At the iteration at discrete time t, the winning neuron w_j moves towards the input pattern (Figure 3.6), and the two neighboring neurons w_{j-1} and w_{j+1} in its Gaussian neighborhood move in smaller steps. The goal is to train the net until the topology is stable.

For each position update of a node the directional convergence of orientation vector is also achieved.

SOFMAT Algorithm Summary

- **Input**: A set of nodes N_y strings each of which is made of N_x nodes, iteration number and similarity matrix.
- Initialization of weight vector by 3.3
- Compute the quantity by Eq. 3.2 :

  $\rightarrow$ *winning neuron* $P(I)$
- Compute the quantity by 3.7 using 3.4, 3.5 3.6:

  $\rightarrow$ *weight update matrix* $w_j(t)$

  $\Rightarrow$ update is achieved for position and for orientation.
- Compute cost function for position and orientation respectively:

  $\forall i, j \in ROI$:

  $C(i,j) = (w_{ij}(n,1) - w_{ij}(n-1,1))^2 + (w_{ij}(n,2) - w_{ij}(n-1,2))^2$

  $C = C./max(C(:))$

  $\forall i, j \in ROI$:

  $A(i,j) = 1 - (w_{ij}(n,3) \times \mathrm{w}_{ij}(n-1,3) + w_{ij}(n,4) \times \mathrm{w}_{ij}\ (n-1,4))$

  $A = A./max(A(:))$
- Terminate the iterations if convergence is reached;
- Store next winning neuron into SOFMAT,
- Otherwise, increase the iteration and repeat steps 1 through 4.
- **Output:** The resulting topology $\leftrightarrow$ The converging weight matrix that includes both the position and orientation information.

Following the three processes of the unsupervised learning method, taking into account both the position and the direction of a candidate node, SOFMAT enables the determination of neural fiber tracts having similar diffusivity. The updated neighborhood helps to compute the proper neighbor of each winning neuron, which enables the algorithm to calculate the neural paths with respect to the underlying diffusivity.

3.5 Experimental Methods

The number of inputs is determined by the image dimensions, which is 150x150 pixels in PISTE. The number of strings and the number of nodes in each string have been changed between $2-80$, and $50-3200$ respectively for experimenting the convergence behavior of different PISTE topologies. The learning rate in Eq. 3.7 was set as 0.1, a typical rate for safe and stable convergence in the expense of slow learning and increased risk of local minima. Each individual PISTE pattern is examined for a number of iterations. For linear and linear break PISTE patterns, 500 iterations were sufficient. For the spiral trajectory the number of iterations were 6000 as expected. By varying iterations, the best match and the determination of the most reliable track is aimed. The more complex the investigated pattern becomes, the more iterations are needed. This is a natural characteristic of a self-organizing network. The main constraint here is the convergence. In each experiment the convergence is checked upon both the position and orientational training results. More detailed explanations and their discussions on experiments and their results are presented in Sections 4 and 5. The tracking results for SOFMAT are shown on four exemplary synthetic data sets. The PISTE trajectories described in Section 2.2 were selected for the evaluation and comparison purposes when GTRACT and SLT methods were employed in the literature [47]. Both GTRACT and SLT are diffusion tensor fiber tracking suites like SOFMAT. The main difference is that these suites include streamline tracking tools. These fiber tracking methods include a guided tracking tool that integrates apriori information into a streamline algorithm. SOFMAT in contrast enables the tracking by detecting and following the orientation of the weighted neighbors. Especially the spiral trajectory which is known to be problematic for fiber tracking methods is also analyzed with SOFMAT. The reconstructed tracts are represented in the Results section, overlaid on the $T2$ weighted MR images or FA maps of the reconstructed tract.

4. Results

4.1 Experimental Scenarios and Targets

In this study, the linear, linear break, orthogonal crossing, and spiral PISTE data sets each of them with individual FA were examined with SOFMAT. Varying FA values give information about the anisotropy and as a result about the anatomy of the tissue investigated. A change in the FA map shows clues about the investigated trajectory. In PISTE, images are created on homogeneous anisotropic background, and decreasing anisotropy along tracts is applied. Therefore, the FA maps serve as filters where the routinely applied homogeneous anisotropic background can be extracted from the image. This process also acts as a noise removal highlighting the diffusion pattern. The eigensystem of D (Eq. 2.23) is determined by principal component analysis (PCA) [1, 58, 68], the principle diffusion direction is interpreted graphically in Figure 4.1. The entire DT resource is investigated with the proposed SOFMAT method. The search process of the pattern in the selected limits is completed in examining the eigenvectors of each pixel based on the predefined similarity measure. This examined data set sample might be a whole image data or a single ROI. In this study the trajectories are not separated into ROIs, they are examined on whole. The details of the investigated geometries are:

4.1.1 Linear Trajectory with and without Break

The linear trajectory is a straight-forward linear tract (Figure 4.1a). Its background is homogenously anisotropic. One has a complete break at the tract (Figure 4.2). Along the length of the tract, its FA is linearly decreasing. The reconstructed tracts are plotted over the FA map of the investigated linear fiber trajectory (Figure 4.1). SOFMAT resolves the break on the linear break trajectory (Figure 4.2-4.3), and it successfully calculates and reconstructs the tracts on the investigated fiber and not

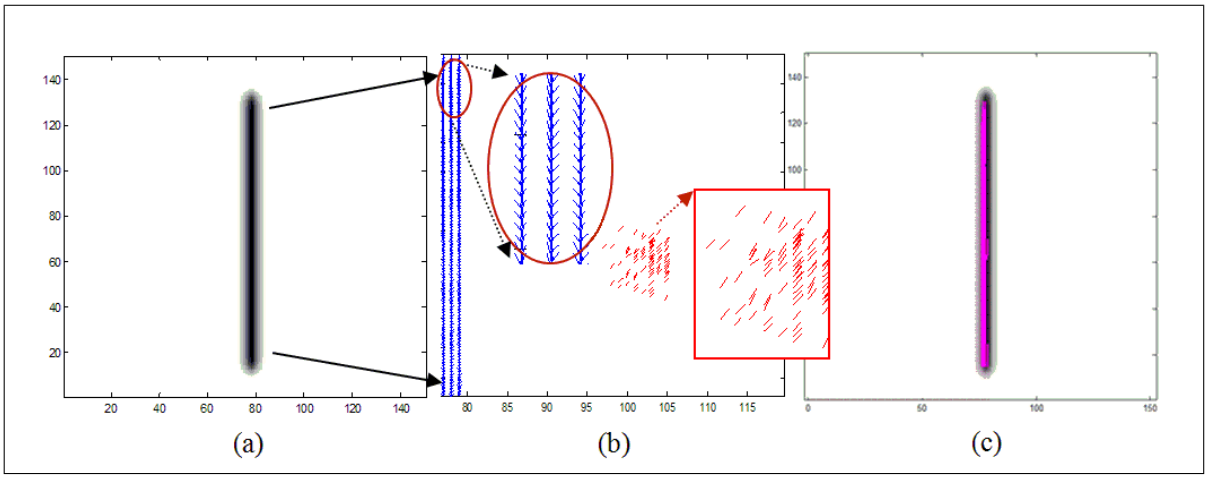

Figure 4.1 Linear PISTE trajectory. a) T2 weighted image; b) Input corresponding to the computed eigenvectors (blue). Initial weights w_{j0} are seen in red. c) Pink tracts on the T2 weighted image are SOFMAT's implementation results.

on the break (Figure 4.3).

4.1.2 Orthogonal Crossing Trajectory

This PISTE trajectory is a crossing sample of two fibers intersecting each other at a right angle. The FA values of each of these two orthogonal linear tracts have a slight difference as represented in the orthogonal elements in diffusion tensor image (Figure 4.4). The difference observed here is fibers with higher and lower FA values. SOFMAT reconstruction is displayed in Figure 4.5. Here, the network has converged with 40x20 nodes in 500 iterations.

4.1.3 Spiral Trajectory

The spiral trajectory of PISTE is an in-plane spiral tract overlaid on a homogenous isotropic background. It has a high FA value. Here, not only the noise-free sample is investigated by SOFMAT but also the curvy trajectory is examined for SNR values of 30 and 15. Spiral tracts are especially problematic for streamline tractography [1, 29], because curvy trajectory cannot be reconstructed accurately by this method. So it is not able to follow the relatively high curvature of the fiber. SOFMAT, however, has

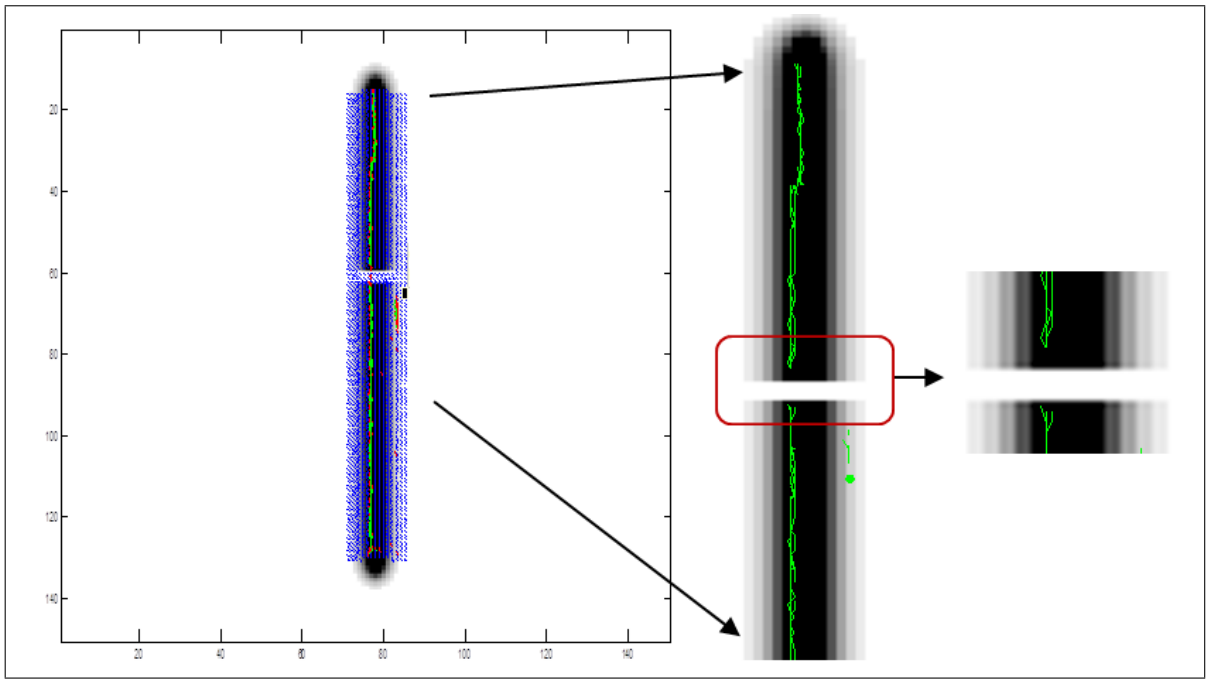

Figure 4.2 Linear Break Trajectory. Eigenvectors representing the diffusivity are superimposed on $T2$ image in blue. SOFMAT results with single string trial are seen in green (right). The gap in the middle of the tract is zoomed to give idea about the implementation result of the algorithm.

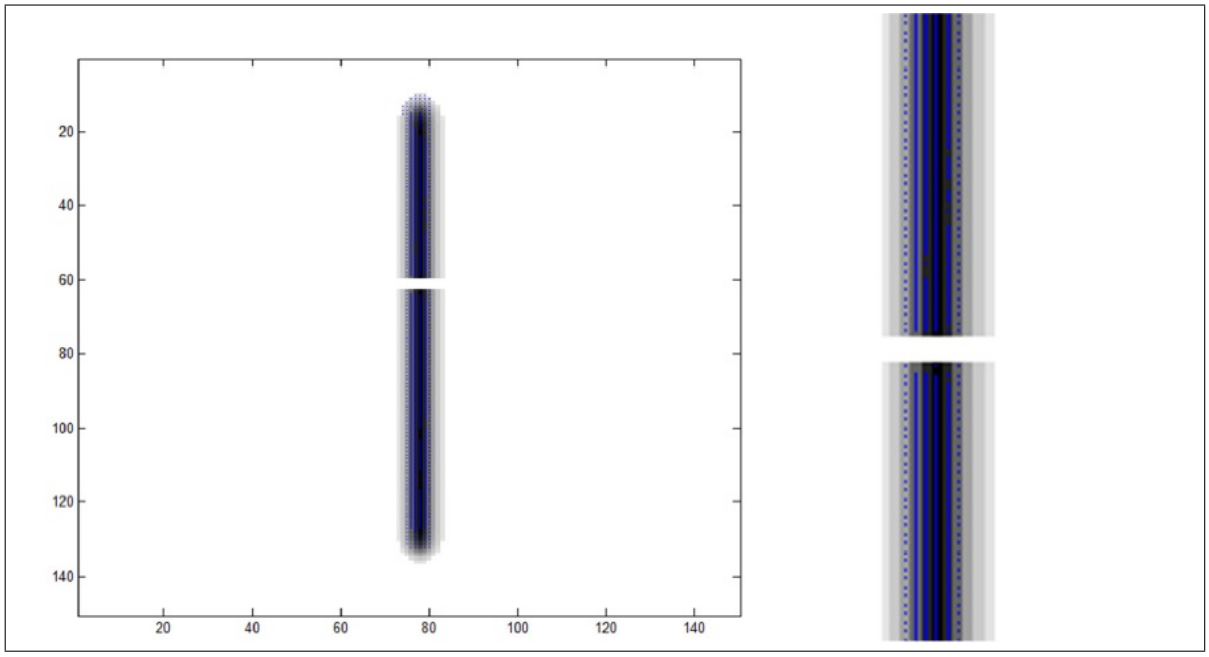

Figure 4.3 Linear Break Trajectory with multiple strings. SOFMAT results are seen in blue. The trajectory and the gap in the middle of it is determined by SOFMAT as represented.

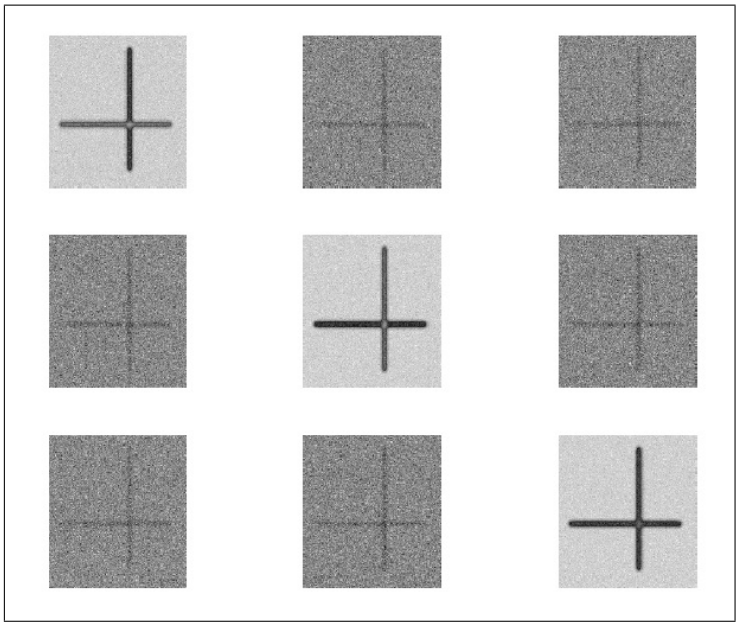

Figure 4.4 Diffusion tensor representation of the Orthogonal PISTE Trajectory. The different diffusivities for this geometry are seen on the diagonal images: Upper left : D_{xx} -the anisotropy of D in x direction and in the middle : D_{yy} -the anisotropy of D in y direction.

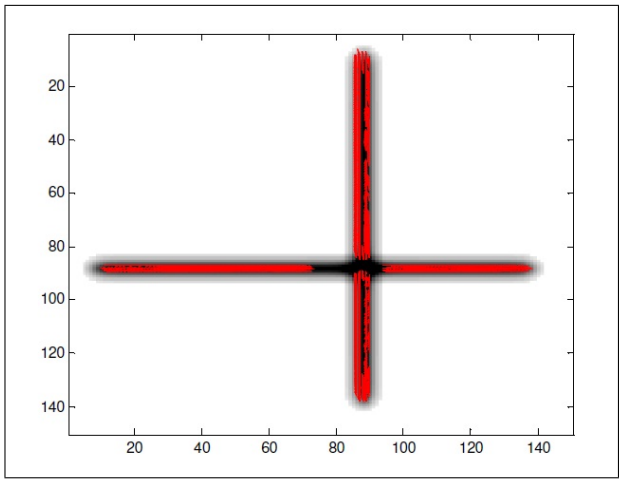

Figure 4.5 The SOFMAT result superimposed on $T2$ images for orthogonal crossing trajectory. The tracts are defined along the paths through the total trajectory. Both of the orthogonal tracts are reconstructed completely. SOFMAT determines the proper path and the expected diffusivity in horizontal tract and vertical tract as seen in Figure 4.4 respectively in D_{xx} and D_{yy}.

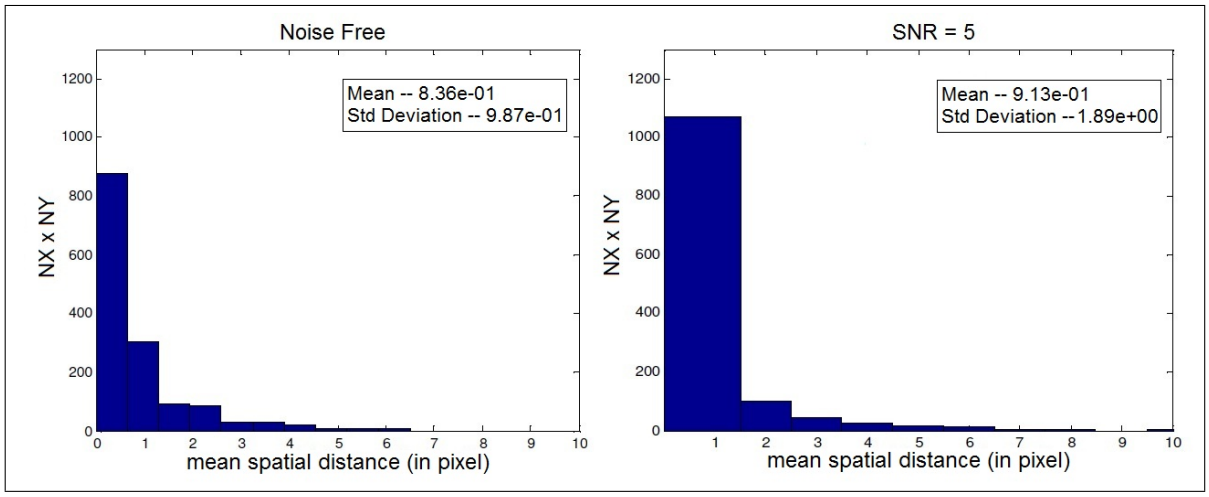

Figure 4.6 The SOFMAT results are investigated, and the determined neighborhood's coordinates and their related calculated eigenvectors are evaluated. The histogram shows the similarity of the original input and the SOFMAT's reconstructed tract for orthocrossing trajectory: noise free (left) and SNR=5 (right). The angular cost function results inform that the input and the output are nearly the same. Here, the input pattern is 150x150, where in both cases noise free and SNR=5, the parameters N_x and N_y are 80 and 40 respectively.

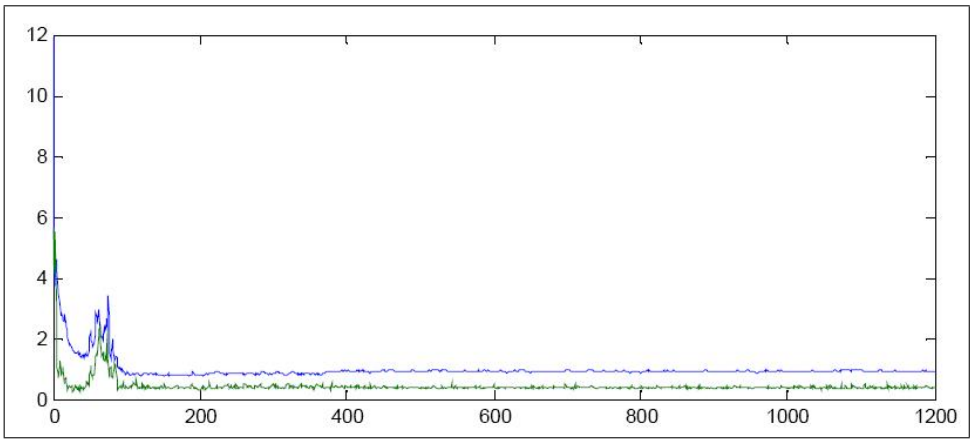

Figure 4.7 Cost function representations of SOFMAT implementation at the end of 1200 iterations. Both the the spatial (blue) and the angular (green) cost functions are calculated, and observed. The network is converged.

the ability to follow the curvature. The reconstruction results are presented in Figure 4.8.

Table 4.1
The mean tracking errors (in mm) of SOFMAT reconstruction of spiral trajectory in Figure 4.8.

SOFMAT		
	Spatial	Angular
Noise free	0.699	0.1151
SNR = 30	0.743	0.1127
SNR = 15	1.611	0.3416
SNR = 5	6.298	0.5087

4.1.4 Crossing Trajectory: Curve Crossing vs. Kissing Trajectory

The curve crossing and kissing trajectories of PISTE are in-plane crossing tracts overlaid on a homogenous isotropic background. They both are crossing trajectories in general. The PISTE trajectories differ in their type of crossing: Curve crossing trajectory is a PISTE sample with two fibers intersecting each other building a local curve crossing trajectory. Kissing trajectory on the other hand is a PISTE sample with two fibers kissing each other building a local crossing curvature.

The kissing trajectory is comprised of two elliptical tracts overlayed on an isotropic, homogeneous background.The FA values of each of these two fiber tracts in each crossing PISTE sample have a slight difference. The difference observed in Figure 4.9.a and in Figure 4.10.a reflects fibers with higher and lower FA values in each of these samples. The presented curve crossing fiber tract sample is visually identical to the kissing tract. The $T2$ values for the tract and background for the curve crossing and kissing trajectories of PISTE are assumed to be the same as white matter (65 ms) and grey matter (95 ms) at $1.5T$, respectively [63]. Three datasets are available with varying levels of added noise.

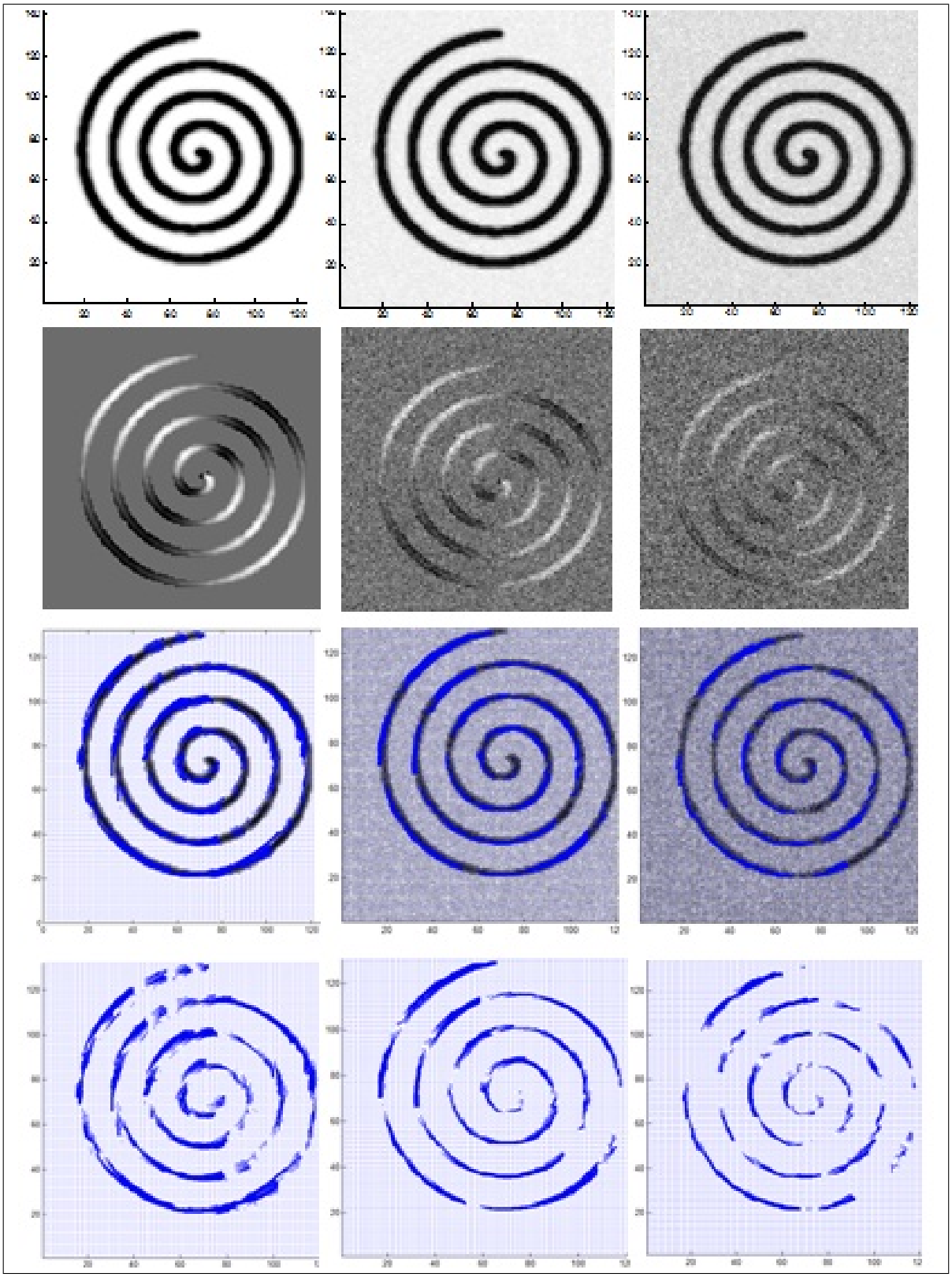

Figure 4.8 The spiral trajectory results are represented. a) Upper row: $T2$ weighted images; from left to right: Noise free $T2$, SNR=30; SNR=15. b) FA images of each input data. c) Third row: SOFMAT results superimposed on respective T2 weighted images. d) SOFMAT reconstructions exclusively. In all examinations, the input pattern is the T2 weighted image of spiral trajectory with input matrix size of 150x150. In order to compare SOFMAT's results, the network in all of the three cases has 50 strings, where number of iterations is 6000, and unique in all three exams.

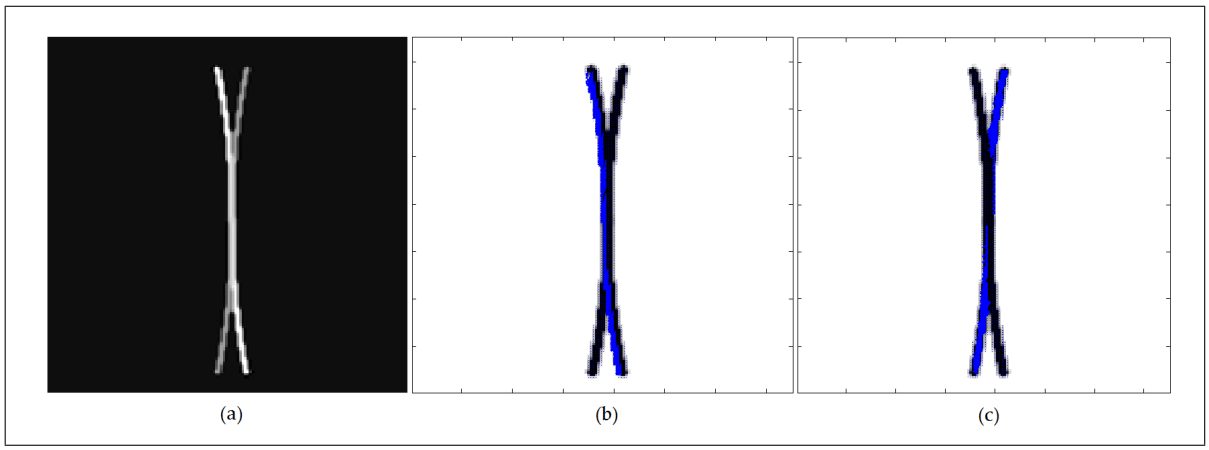

Figure 4.9 The curve crossing trajectory results are represented for each of the two elliptical tracts with different FA values. a) FA map representation, b) and c) SOFMAT results superimposed on $T2$ weighted image. The tracts intersecting each other resulting a local curve crossing trajectory is identified by SOFMAT.

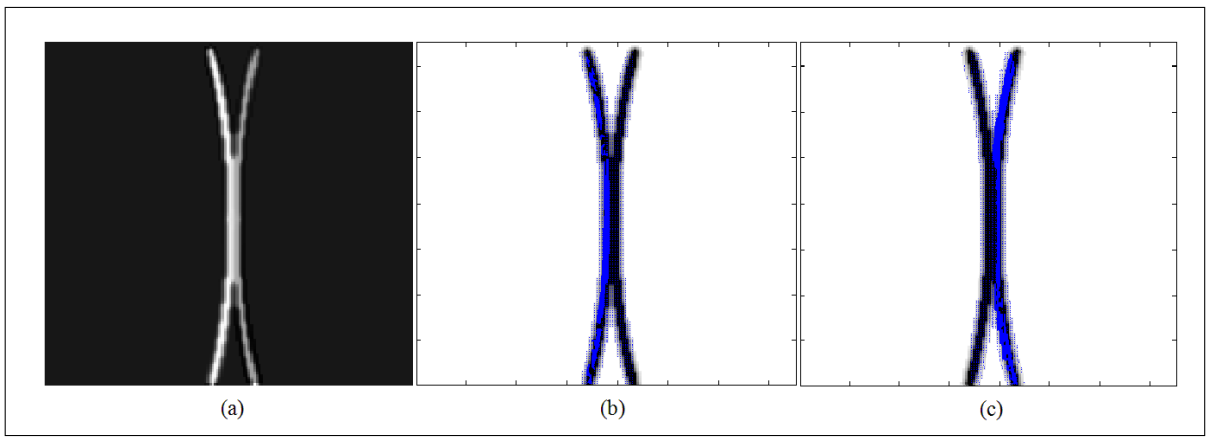

Figure 4.10 The kissing trajectory result of SOFMAT is represented. Unlike the curve crossing sample the elliptical tracts have a different propagation here. a) FA map representation, b) and c) SOFMAT reconstructions of the tracts with higher and lower FA values respectively. The SOFMAT results are superimposed on $T2$ weighted image.

SOFMAT tracking results for both curve crossing trajectory (Figure 4.9) and the kissing trajectory are represented (Figure 4.10). SOFMAT identifies the two elliptical tracts as intersecting in the curve crossing and as slightly touching each other in the kissing trajectory sample.

4.1.5 General Aspects of Phantom Implementation Results

The proposed SOFMAT algorithm is compared with the two well-known fiber tracking suits, GTRACT [47] and SLT [1] using PISTE data set as a benchmark. The

tracking results for the three algorithms were compared qualitatively and quantitatively. As indicated in the reference papers Lori et al. (2002) [51] and Lazar et al. (2003) [49], the error in fiber tracking is proportional to the square root of the distance along the track. The evaluation of GTRACT algorithm has been performed regarding the predefined error definition as in Lori et al. (2002) [51] and Lazar et al. (2003) [49] [47]. Also in this work, the error is computed based on distance measure as in the definition in the literature. In GTRACT [47], the tracking error was accessed on the linear trajectory, and the orthogonal crossing trajectory. For that reason, error of SOFMAT is computed for the two phantom trajectories, the linear and the orthogonal crossing and computation results are presented in Table 4.2 and 4.3. Aside from the linear, linear break, orthocrossing trajectories mentioned in [47] spiral trajectory is also investigated in this study.

The results for all the three tracking tools are represented in Tables 4.2 and 4.3 for all the existing linear and orthogonal PISTE trajectories respectively. The mean tracking errors in STL, GTRACT and SOFMAT for linear PISTE trajectory with an SNR of 30 are 0.63 mm, 0.60 mm and 0.46 mm respectively (Table 4.2). With an SNR of 5, again for the linear trajectory, the tracking errors for STL, GTRACT and SOFMAT are 1.40 mm, 0.70 mm, and 0.56 mm respectively (Table 4.2). The mean tracking errors in STL, GTRACT and SOFMAT for orthogonal crossing phantom with an SNR of 30 are 0.675 mm, 0.65 mm and 0.46 mm respectively (Table 4.3). The mean tracking error in STL and GTRACT for orthogonal crossing phantom (SNR=5) are 1.45 and 0.7 mm respectively. SOFMAT's tracking error for SNR=5 for ortho-crossing phantom is 0.65 mm (Table 4.3). Here, the SOFMAT parameters N_x and N_y are in each experiment 80 and 40 respectively. The parameters are assigned based on the network's convergence status. The updated network parameters are given in detail in Table 4.6.

To observe the effectiveness of the ANN based algorithm, the cost function convergence is detected as SOFMAT weights are stabilized (Figure 4.7). The SOFMAT tracking results of an uncertainty region namely an orthocrossing trajectory is also presented in Figure 4.5.

Table 4.2
The tracking errors (in mm) of the three tracking tools for linear trajectory.

	STL	GTRACT	SOFMAT
SNR = 30	0.63	0.60	0.46
SNR = 15	0.90	0.65	0.48
SNR = 5	1.40	0.70	0.56

Table 4.3
The tracking errors (in mm) of the three tracking tools for orthogonal crossing trajectory.

	STL	GTRACT	SOFMAT
SNR = 30	0.675	0.65	0.46
SNR = 15	0.875	0.66	0.48
SNR = 5	1.45	0.70	0.65

For each of the investigated trajectory, the network's parameters are methodically and carefully determined. The determination of parameters effect the phases of the network and its ability to converge safe and stably. As mentioned previously, each individual PISTE pattern is examined for a number of iterations. The aim of varying iterations is to find the best match and so to determine the most reliable tract. The more the investigated pattern gets complex, iteration numberincreases. This also explains why the spiral trajectory's iteration number (= 6000) was the highest among all the trajectories. This is a natural characteristic of a self-organizing network.

In each experiment the convergence is checked upon both the position and orientational training results. Here, the orthogonal crossing trajectory with 150x150 original input size is selected as sample. In the Tables 4.4, 4.5, 4.6, various network parameter selections and their results are represented. First, a network with 2 strings created from 50 to 200 nodes is analyzed. The mean spatial distance between the known values of the input pattern and those calculated with SOFMAT as output vary from 5.7429 to 1.819 pixels. In all of these cases the iteration number is kept constant with 500 steps. As expected, with increased number of strings the trajectory is more precisely

determined (Table 4.5, 4.6).

Table 4.4
The validation results of the SOFMAT implementation. The orthogonal crossing trajectory is selected as sample. Here, analysis results for 2 strings case are shown.

Node x String	Mean Spatial Distance	Angular Norm
50 x 2	5.7429	0.1206
100 x 2	3.5785	0.0999
150 x 2	2.2843	0.1003
200 x 2	1.8195	0.0965

Table 4.5
The validation results of the SOFMAT implementation for orthogonal crossing. A wider network for orthogonal crossing trajectory is investigated and represented.

Node x String	Mean Spatial Distance	Angular Norm
20 x 20	8.17	0.0923
25 x 20	3.3412	0.0943
30 x 20	2.8286	0.0883
40 x 20	2.1506	0.0910
60 x 20	1.7862	0.0917

4.2 Human Data

The real DTI images used in this study are scanned on Philips Scanner, Achieva in Istanbul Medical School Department of Neurology. The voxel size of the MR images is 1.75mm x 1.75mm. The number of diffusion volumes is 34, where the number of slices is 60. The repetition time TR is 9615.95 ms, and echo time TE is 80.261 ms with a flip angle of 90 degrees. Slice thickness and spacing are both 2 mm. The image size is 128 x 128. The tracking results of the proposed unsupervised learning tracking SOFMAT algorithm is shown on a healthy human brain data. The reconstructed tracts

Table 4.6
The validation results of the SOFMAT implementation for orthogonal crossing with updated network parameters.

Node x String	Mean Spatial Distance	Angular Norm
20 x 40	1.49455	0.0996
40 x 40	1.1065	0.0971
60 x 40	1.0391	0.0969
80 x 40	0.8346	0.0885
100 x 40	0.6577	0.0330
150 x 40	0.8480	0.0890
200 x 40	0.4263	0.0415
250 x 40	0.3729	0.0436
300 x 40	0.3603	0.0504

are represented in Figure 4.11 and 4.12, superimposed on the T2 weighted MR images or FA maps of the reconstructed tract.

4.2.1 General Aspects of Human Data Results

In this study, DTI images are investigated based on the proposed weight updated unsupervised learning algorithm SOFMAT. Analysis is done on normal healthy tissue. Varying FA values give information about the anisotropy and as a result about the anatomy of the underlying tissue. A change in the FA map shows clues about the investigated trajectory as seen in Figure 2.8. The eigensystem of D (2.23 and 2.24) is determined by principal component analysis (PCA) [4, 68], the principle diffusion direction with thresholded FA map is interpreted graphically in Figure 2.8. The search process of the pattern in the selected limits is completed in examining the eigenvectors of each pixel based on the predefined similarity measure. This examined dataset sample might be a whole image data or a single ROI.

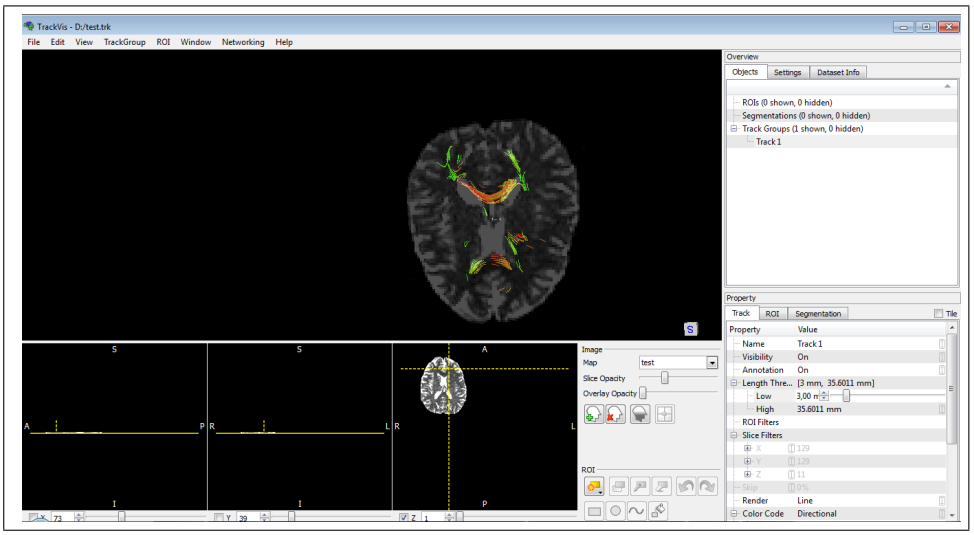

Figure 4.11 Investigated healthy brain image. SOFMAT results visualized in TrackVis. Genu and splenium of the corpus callosum are represented. SOFMAT parameters are $N_x = 15$ and $N_y = 50$.

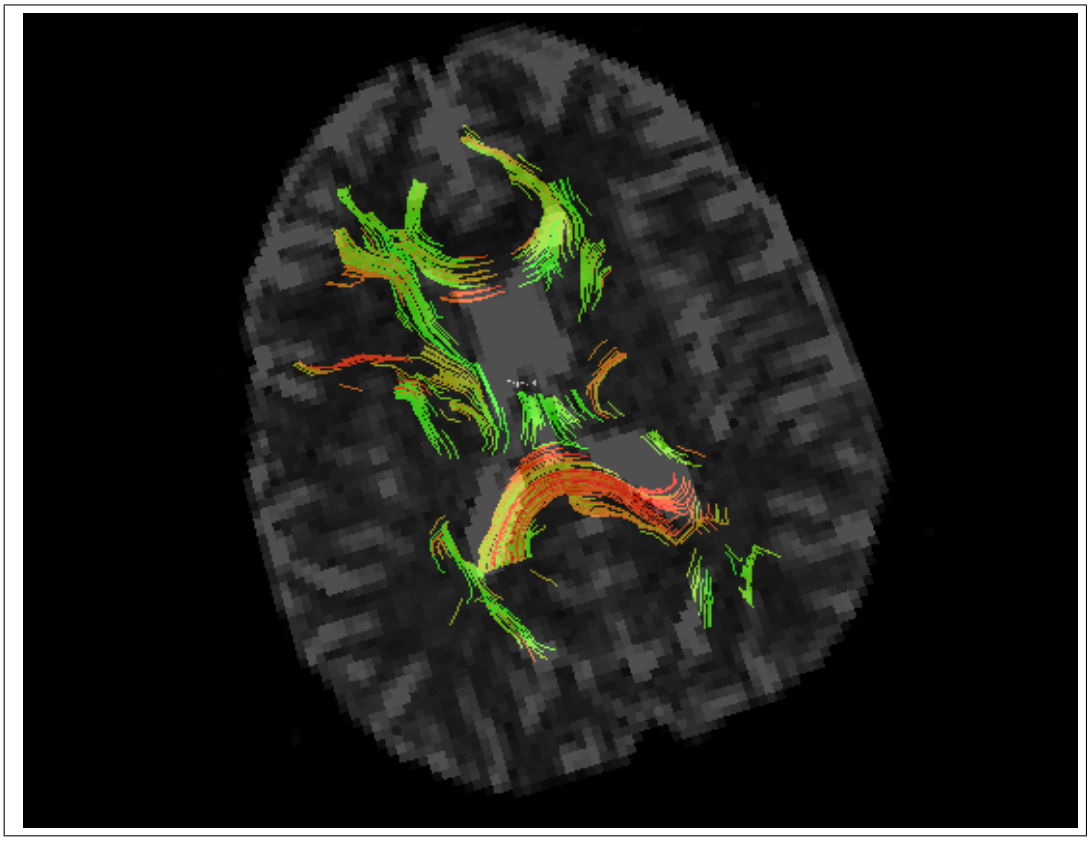

Figure 4.12 Here the multi-string results are superimposed on T2-weighted image. SOFMAT multi-string parameters are $N_x = 50$ and $N_y = 50$.

DTI tractography entails propagation of fibers along the path of greatest diffusivity. TrackVis enables visualization of calculated SOFMAT results. Coloration of fibers then allows the investigation of specific ROIs. SOFMAT enables to detect tract distributions in real brain. According to the investigated ROI, the coloration by visualization raise the anatomy like the genu and splenium seen in Figure 4.11 and 4.12.

5. Discussion

Mapping the brain's white matter noninvasively is possible through proper analysis of DTMR images. The algorithms proposed for WM mapping and fiber tractography are to be examined by synthetically simulated datasets for accurate validation. In this study a common synthetic DT data set namely PISTE, which is specially generated for verification purposes of DT and tractography algorithms, is used for verification and validation. One of the main constraints in the accuracy of the mapping results is the determination of intersecting fiber tracts in uncertainty regions. In DTI literature these intersecting regions generate a critical tracking problem. Providing a solution for identification of the orientations of the brain fibers in these uncertainty regions in diffusion tensor analysis is of great importance [4, 16]. Methods and updates are to be researched to define these uncertainty regions. Streamline Tractography (SLT) is recalled as an accepted basis method for diffusion tensor tractography (DTT). For that reason, SLT is one of the algorithms selected for comparison with SOFMAT (Table 4.2, 4.3). Secondary DTT algorithm chosen for evaluation is the GTRACT software implementation. The SLT uses the principle eigenvector, e_1, to compute an Euler's method approximation to the parameterized tract [1, 29].

In this study, we proposed a tracking tool for detect ingreal WM fibers later as a future study according to unsupervised learning method SOFM. The main idea of SOFMAT is to track the fibers according to unsupervised learning while keeping the structural information of the underlying tissue. The methodology is applied and examined firstly on computer simulated trajectories PISTE for verification and validation of the algorithm.

The proposed fiber reconstruction method SOFMAT clarifies the diffusivities in the previously mentioned uncertainty regions (Figure 4.1, Figure 4.3 and Figure 4.8). Quantitative results are listed in Table 4.2 and 4.3 with respect to well accepted tractography techniques [1, 29, 47]. The Figures in Result Section are represented to give an

idea of how (well) the SOFMAT results match the input patterns.The method is tested with varying SNR values and also in low anisotropy regions. Low anisotropy regions are studied more intensely focusing on the problematic crossings on the phantoms. The fractional anisotropy (max. FA=1) represents the degree of anisotropy, in other words the deviation from isotropic diffusion (FA=0). The grey matter in the brain is nearly isotropic (0.37>FA>0.15). In uncertainty regions, it is hard to define the direction of principal diffusivity. Therefore the detection of fibers in regions having low fractional anisotropy is an advantage of the proposed method because aside from grey matter, low anisotropy regions are uncertainty areas or injured regions. Optimizing the cost function and neuron selection, the algorithm is able to detect small tract changes and curvy trajectories.

Fiber tracking in SOFMAT begins by identifying seed voxels to be used as potential starting positions for the reconstructed fibers. Based on the predetermined eigensystem of the sample trajectories, fiber tract is estimated within each voxel regarding to the diffusivity defined by this eigensystem. Here, the knowledge in diffusion literature suggests that the eigensystem defines the diffusivity [1, 29]. Each node (neuron) in the region of interest (ROI) is considered as part of a potential fiber tract. The computed winning neurons define the possible nervetract a fiber can follow with respect to both the coordinate and the directional information the winning neurons. In other words, a winning neuron determines the newly gained voxel to the tract in terms of its coordinate and direction. The estimation follows by evaluating each node's neighboring function in terms of the similarity criteria.

The novel algorithm SOFMAT is being evaluated throughout the study. The validation study performed on PISTE gives promising results, and they have been compared to the well-known SLT method and the GTRACT algorithm. In the literature, as it has been represented in Cheng et al. (2006) [47] by GTRACT evaluation, the error is investigated along the resulting tract and quantitative results are given in Table 4.2 and 4.3. SOFMAT is able to handle fiber crossings and also the spiral trajectory. SOFMAT results to highlight to propagation of fibers through the intersecting and curvy regions are represented in Figures 4.1, 4.2, 4.3, 4.5, 4.8, and also in

the spatial and angular cost functions (Figure 4.7). The minimization of the error is successfully managed where the characteristics can be tracked in related cost function of the network. The increasing number of neurons and iterations selected in the SOM implementation result more reliable tractography outputs (Table 4.4, 4.5 and 4.6).

Investigating samples with both varying noise and different geometry is important for evaluation, because the deviation from the original fiber path is caused mainly by the noise. The relationship between the tracking error to SNR is acceptable in all examinations. Also dependency on the geometry is seen (Figure 4.1 and Figure 4.8). Considering that every trajectory in PISTE has a different diffusivity characteristics, it is meaningful that the cost functions representing the fiber determination performance for linear and orthocrossing geometries vary from each other. The SOFMAT algorithm improves the performance of the fiber tracking even in the presence of noise discussed in Tables 4.2 and 4.3. SOFMAT also allows tracking branching fibers. In conclusion, SOFMAT is able to describe two or more fiber tracts simultaneously, and to reconstruct tracts in uncertainty regions. While SNR decreases for an investigated pattern, the spatial and angular cost function reflects this change (Figure 4.7. SOFMAT, on the other hand, does not lose the fiber tractography in relatively low SNRs.

The SOFMAT method gives promising results, compared to the traditionally implemented and well accepted tractography algorithms mentioned above (Table 4.2 and 4.3). SOFMAT is applied to healthy human DT images. The SOFMAT application parameters such as learning rate, neighborhood size are selected as the same values which were optimized in the simulation studies. It has been observed that the well-known fibers can be estimated by the use of the proposed method. The results of SOFMAT are in agreement with the physiological fiber pathways. For instance, fibers that are estimated in the white matter do not elongate to other tissue types such as the CSF and grey matter (Figure 4.12).

6. Conclusion and Future Work

In this thesis, the interest has been focused on generating an algorithm for fiber tract determination. The study represents a novel approach namely SOFMAT for fiber tracking purposes in diffusion tensor analysis. The algorithm is based on unsupervised learning in artificial neural networks. As an alternative to the existing methods, SOFMAT is also effective in low anisotropy regions. Also, unlike some DTT studies established with PISTE [59, 69], the presented SOFMAT study provides performance evaluation other than just visual inspection. The error analysis of the SOFMAT results compared to the existing methods gives improved tract determination and follow-up. In crossing regions with intersecting fiber distributions and varying SNR values, SOFMAT is able to define the predetermined fiber paths successfully with a standard deviation of $(0.8-1.9)$ mm depending on the trajectory and the SNR value selected. The results illustrate the capability of SOFMAT to reconstruct complex fiber tract configurations. Due to higher level connectivity concerns SOFMAT configurations could be modified, and the network might be forced to estimate any tracts in high noise level or extremely curving trajectories, even in the presence of disconnected tracts.

As some of the white matter tracts elongate throughout the whole brain, the SOFMAT algorithm can be implemented on the full DT images. The computational demand of the full data implementation is higher than the need for ROI applications. Thus, distributed computing based on parallel working central processing units (CPU) should be used to estimate the relevant DTI tracts in reasonable time. The SOFMAT algorithm can be modified in such a way that the extraction of the fibers can be performed by different CPUs.

With the usage of multiprocessor computers, real-time full brain tractography analysis can be performed even in the MR control room. The advancement in speed of SOFMAT may enable radiologists, medical doctors, and experts in the field to visualize and analyze the information content in the daily usage.

The proposed algorithm can be implemented on neurological disorders for the estimation of pathologies, detection of white matter alterations, and therapeutical planning of neurological disorders. Moreover, appropriate DTI tracking enables neurosurgeons efficient information about WM tracts for surgical planning.

APPENDIX A. Academic Works - Bibliography

A.1 Book Chapters

1. Duru, D.G. and M. Özkan, "Chapter 3: Determination of Neural Fiber Connections Based on Data Structure Algorithm," *Data Structure and Software Engineering Challenges and Improvements*, Edited by James L. Antonakos, Pages 4252, Print ISBN: 978-1-926692-97-5, eBook ISBN: 978-1-4665-6260-8, DOI: 10.1201/b13126-5, Apple Academic Press, Oct 2012.

2. Duru, D.G. and M. Özkan, "Chapter 4: Information and Data Architecture," *Advances in Information Technology Research and Application: 2011 Edition*, ISBN 978-1-4649-2074-5, Scholarly Editions Press, Atlanta, 2011.

3. Göksel Duru, D., "A Hebbian Learning Approach for Diffusion Tensor Analysis and Tractography," *New Advances in Machine Learning*, ISBN 978-953-307-034-6, InTech Press, p. 345-356, 2010.

4. Göksel Duru D., and M. Ozkan, "Generating Simulated DT-MRI Dataset," *Encyclopedia of Healthcare Information Systems, Information Science Reference*, ISBN 978-1-59904-889-5, Publisher Medical Information Science Reference IGI Global, p. 623-630, 2008.

A.2 Peer Reviewed Journal Papers and Full Paper Proceedings

1. Göksel Duru, D., and M. Özkan, "Application of Self-Organizing Artificial Neural Networks on Simulated Diffusion Tensor Images," *Mathematical Problems in Engineering*, vol. 2013, Article ID 690140, 13 pages, 2013. doi:10.1155/2013/690140

2. Göksel Duru, D., and M. Özkan, "Determination of Neural Fiber Connections Based on Data Structure Algorithm," *Computational Intelligence and Neuroscience*, vol. 2010, Article ID 251928, 2010. doi:10.1155/2010/251928

3. Göksel Duru, D., and M. Özkan, "Analysis of Diffusion Tensor Eigensystem Based on an Artificial Neural Network Approach," 28th International Physics Congress, Bodrum, 6-9 September 2011.

4. Göksel Duru, D., and M. Özkan, "Implementation of an Artificial Neural Network Based Algorithm for Diffusion Tensor Tractography," 16th Annual Meeting of the Organization for Human Brain Mapping, Palau de Congressos de Catalunya, Barcelona, 6-10 June 2010.

5. Göksel Duru, D., and M. Özkan, "Determination of Neural Fiber Connections Based on Data Structure Algorithm," 7th International Symposium on Noninvasive Functional Source Imaging of the Brain and Heart 7th International Conference on Bioelectromagnetism, Engineering Faculty of Rome, Rome, Italy, 29-31 May 2009.

6. Göksel Duru, D., and M. Özkan, "Fiber Tracking Based on Unsupervised Learning," Proceedings of NER '09, the 4th International IEEE/EMBS Conference on Neural Engineering, p. 566 - 569, 2009.

7. Göksel Duru, D., and M. Özkan, "Self Organizing Feature Maps for the Fiber Tracking in Diffusion Tensor MR Images", Proceedings of the 4th Institution of Engineering and Technology International Conference on Advances in Medical, Signal and Information Processing MEDSIP 2008, p. 1-4, 2008.

8. Göksel Duru, D., and M. Özkan, "SOM Based Diffusion Tensor MR Analysis," 5th International Symposium on Image and Signal Processing and Analysis ISPA 2007, p. 403-406, Digital Object Identifier 10.1109/ISPA.2007.4383727, 2007.

9. Göksel Duru, D., and M. Özkan, "Fiber Tracking: A Recursive Stack Algo-

rithmic Approach," Proceedings of 29th Annual International Conference of the IEEE Engineering in Medicine and Biology Society in conjunction with the Biennial Conference of the French Society of Biological and Medical Engineering (SFGBM), p. 315 - 318, 2007.

10. Göksel Duru, D., and M. Özkan, "Simulated Dataset for Verification Validation of DT-MRI Analyzing Tools," Proceedings of 28th IEEE EMBS Annual International Conference, New York, p. 1924-1927, 2006.

11. Göksel Duru, D., and M. Özkan, "Simulated Diffusion Tensor MR Imaging (DT-MRI) Dataset for Verification and Validation of DT Analyzing Tools," Proceeding Book of 5th International Conference on Advanced Engineering Design - AED 2006, vol. 5, pp.122-129, 2006. ISBN number 80-86059-44-8

A.3 Peer Reviewed Abstract Proceedings

1. Goksel Duru D., and M. Ozkan, "Diffusion tensor tractography based on linked list algorithm," CARS 2007 Computer Assisted Radiology and Surgery, Berlin, Germany, June 27 - 30, 2007. Accepted paper to the Joint Congress of CAR / ISCAS / CMI / CAD / EuroPACS

2. Goksel Duru D., and M. Ozkan, "A synthetic diffusion tensor dataset generation: verification validation of DT-MRI analyzing tools," CARS 2007 Computer Assisted Radiology and Surgery, Berlin, Germany, June 27 - 30, 2007. Accepted paper to the Joint Congress of CAR / ISCAS / CMI / CAD / EuroPACS

3. Goksel Duru D., and M. Ozkan, "Diffusion Tensor MR Imaging: Simulated Dataset for Verification and Validation of DT-MRI Analyzing Tools," International Workshop on Image Analysis in the Life Sciences, Theory and Applications, Linz, Austria, 28 February - 2 March 2007.

4. Goksel D., and M. Ozkan, "Towards rapid analysis of diffusion tensor MR imaging," European Radiology, vol. 16(1), p. 286, Feb 2006.

A.4 Peer Reviewed Full-Paper Proceedings (National)

1. Göksel Duru, D., and M. Özkan, "Diffusion tensor fiber tracking based on unsupervised learning - Gözetimsiz Öğrenmeye Dayalı Difüzyon Tensör Yolak Takibi," Proc. 15. National Biomedical Engineering Meeting, p. 1-4, 2010.

2. Göksel Duru, D., and M. Özkan, "Fiber tracking using recursive stack data structure - Özyineli Yığıt Veri Yapısı Kullanılarak Yolak Takibi," 14th National Conference in Biomedical Engineering, p. 1-3, 2009. DOI:10.1109/BIYOMUT.2009.5130350

3. Göksel Duru, D., and M. Özkan, "Bootstrap Application in Diffusion Tensor Imaging - Difüzyon Tensör Görüntülemede Önyükleme Yöntemi Uygulamaları," Proceedings of National Conference of Biomedical Engineering, p.184-186, 2007.

4. Göksel Duru, D., and M. Özkan, "DT-MRG ile Beyin Analizi," Proceedings of National Conference of Biomedical Engineering," p.116-119, İstanbul, 2007.

5. Göksel Duru, D., and M. Özkan, "Difüzyon Tensör MR Analizi: Kardiyak Uygulama," Proceedings of National Conference of Biomedical Engineering, p.225-228, İstanbul, 2007.

6. Göksel D., and M. Özkan, "Difüzyon Tensör MR Analizi Doğrulaması Ve Geçerliliği Amaçli Sentetik Görüntü Seti," Biyomut 2006 - Proc. National Biomedical Engineering Meeting, p. 80-83, 2006.

7. Göksel D., and M. Özkan, "Diffusion Tensor MR Imaging - Difüzyon Tensör MR Görüntüleme,"' Biyomut 2005 - Proc. National Biomedical Engineering Meeting, p. 174-180, İstanbul, 2005.

REFERENCES

1. Basser, P. J., S. Pajevic, C. Pierpaoli, J. Duda, and A. Aldroubi, "In vivo fiber tractography using DT-MRI data," *Magnetic Resonance in Medicine*, Vol. 44, pp. 625–632, 2000.

2. Szafer, A., J. Zhong, A. W. Anderson, and J. C. Gore, "Diffusion-weighted imaging in tissues: theoretical models," *NMR in Biomedicine*, Vol. 8, no. 7-8, pp. 289–296, 1995.

3. Pajevic, S., and C. Pierpaoli, "Color schemes to represent the orientation of anisotropic tissues from diffusion tensor data: Application to white matter fiber tract mapping in the human brain," *Magnetic Resonance in Medicine*, Vol. 42, pp. 526–540, 1999.

4. Bihan, D. L., C. Poupon, A. Amadon, and F. Lethimonnier, "Artifacts and pitfalls in diffusion MRI," *J. Magn. Res. Imaging*, Vol. 24, pp. 478–488, 2006.

5. Lee, S. K., "Diffusion tensor MRI: clinical applications and pitfalls," *Fortschr Röntgenstr*, Vol. 177, pp. 478–488, 2005.

6. Sotak, C. H., "The role of diffusion tensor imaging in the evaluation of ischemic brain injury - a review," *NMR in Biomedicine*, Vol. 15, pp. 561–569, 2002.

7. Haykin, S., *Neural Networks: A comprehensive foundation*, NJ, USA: Prentice-Hall, Inc., 2005.

8. Ciccarelli, O., G. J. M. Parker, C. A. M. Wheeler-Kingshott, G. J. Barker, P. A. Boulby, D. H. Miller, and A. J. Thompson, "From diffusion tractography to quantitative white matter tract measures: a reproducibility study," *Neurolmage*, Vol. 18, pp. 348–359, 2003.

9. Hänggi, P., and F. Marchesoni, "Introduction: 100 years of Brownian motion," *CHAOS*, 2005.

10. Beaulieu, C., "The basis of anisotropic water diffusion in the nervous system - a technical review," *NMR in Biomedicine*, Vol. 15, no. 7-8, pp. 435–455, 2002.

11. Tuch, D. S., *Diffusion MRI of Complex Tissue Structure*. PhD thesis, Massachusetts Institute of Technology, Massachusetts, 2002.

12. Crank, J., ed., *The Mathematics of Diffusion*, Oxford, UK: Oxford University Press, 2004.

13. Kang, N., J. Zhang, E. S. Carlson, and D. Gembris, "White matter fiber tractography via anisotropic diffusion simulation in the human brain," *IEEE Transactions on Medical Imaging*, Vol. 24, pp. 1127–1137, September 2005.

14. Torrey, H. C., "Bloch equations with diffusion terms," *Physical Review*, Vol. 104, no. 3, p. 563, 1956.

15. Stejskal, E. O., and J. E. Tanner, "Spin diffusion measurements: spin echoes in the presence of a time-dependent field gradient," *Journal of Chemical Physics*, Vol. 42, pp. 288–292, 1965.

16. Basser, P. J., J. Mattiello, and D. L. Bihan, "MR diffusion tensor spectroscopy and imaging," *Biophys J*, Vol. 66, no. 1, pp. 259–267, 1994.

17. Basser, P. J., J. Mattiello, and D. L. Bihan, "Estimation of the effective self-diffusion tensor from the NMR spin echo," *J Magn Reson B*, Vol. 103, no. 3, pp. 247–254, 1994.

18. Mori, S., and P. B. Barker, "Diffusion magnetic resonance imaging: Its principle and applications," *The Anatomical Record (New Anat.)*, Vol. 257, pp. 102–109, 1999.

19. Johansen-Berg, H., and T. Behrens, eds., *Diffusion MRI: From quantitative measurement to in-vivo neuroanatomy*, Academic Press, 2009.

20. Mori, S., ed., *Introduction to Diffusion Tensor*, Oxford, UK: Elsevier, 2007.

21. Scollan, D. F., *Reconstructing the Heart Development and Application of Biophysically based Electrical Models of Propagation in Ventricular Myocardium Reconstructed from Diffusion Tensor MRI.* PhD thesis, Johns Hopkins University, Baltimore, Maryland, 2002.

22. Taylor, A. J., "Diffusion tensor imaging: Evaluation of tractography algorithm performance using ground truth phantoms," Master's thesis, Virginia Polytechnic Institute and State University, Virginia, 2004.

23. Kindlmann, G., D. Weinstein, and D. Hart, "Strategies for direct volume rendering of diffusion tensor fields," *IEEE Transactions on visualization and computer graphics*, Vol. 6, pp. 124–138, 2000.

24. Berg, H., *Random Walks in Biology*, Princeton, NJ: Princeton University Press, 1983.

25. Douek, P., R. Turner, J. Pekar, N. Patronas, and D. L. Bihan, "MR color mapping of myelin fiber orientation," *J Comput Assist Tomogr*, Vol. 15, pp. 923–929, 1991.

26. Basser, P. J., and D. L. Bihan, "Fiber orientation mapping in an anisotropic medium with NMR diffusion spectroscopy," *Proc 11th Annual Meeting SMRM, Berlin*, Vol. 15, p. 1221, 1992.

27. Jones, D. K., S. C. R. Williams, and M. A. Horsfield, "Full representation of white matter fibre direction on one map via diffusion tensor analysis," *Proc 5th Annual Meeting ISMRM, Vancouver*, Vol. 15, p. 1743, 1997.

28. Pierpaoli, C., "Oh no! one more method for color mapping of fiber tract direction using diffusion MR imaging data," *Proc 5th Annual Meeting ISMRM, Vancouver*, p. 1741, 1997.

29. Mori, S., B. J. Crain, V. P. Chacko, and P. C. van Zijl, "Three dimensional tracking of axonal projections in the brain by magnetic resonance imaging," *Ann Neurol*, Vol. 45, pp. 265–269, 1999.

30. Conturo, T. E., N. F. Lori, T. S. Cull, E. Akbudak, A. Z. Snyder, J. S. Shimony, R. C. McKinstry, M. Burton, and M. E. Raichle, "Tracking neuronal fiber pathways in the living human brain," *Proc Natl Acad Sci USA*, Vol. 96, pp. 10422–10427, 1999.

31. Jones, D. K., A. Simmons, S. C. R. Williams, and M. A. Horsfield, "Non-invasive assessment of axonal fiber connectivity in the human brain via diffusion tensor MRI," *Magnetic Resonance in Medicine*, Vol. 42, pp. 37–41, 1999.

32. Poupon, C., C. A. Clark, V. Frouin, J. Regis, I. Bloch, D. L. Bihan, and J. F. Mangin, "Regularization of diffusion-based direction maps for the tracking of brain white matter fascicles," *Neurolmage*, Vol. 12, pp. 184–195, 2000.

33. Koch, M., V. Glauche, J. Finsterbusch, U. Nolte, J. Frahm, and C. Buchel, "Estimation of anatomical connectivity from diffusion tensor data," *NeuroImage*, Vol. 13, p. S176, 2001.

34. Tuch, D. S., M. R. Wiegell, T. G. Reese, J. W. Belliveau, and V. J. Wedeen, "Measuring cortico-cortical connectivity matrices with diffusion spectrum imaging," *Proc 9th Annual Meeting ISMRM, Glasgow*, p. 502, 2001.

35. Parker, G. J. M., G. J. Barker, and D. L. Buckley, "A probabilistic index of connectivity (PICo) determined using a Monte Carlo approach to streamlines," *ISMRM Workshop Diffusion MRI: Biophysical Issues. St Malo, France*, March 2002.

36. Jones, D. K., "A least squares continuous diffusion tensor field approximation," *NeuroImage*, Vol. 13, p. S168, 2001.

37. Poupon, C., C. A. Clark, V. Frouin, J. Regis, I. Bloch, D. L. Bihan, and J. Mangin, "Regularization of diffusion-based direction maps for the tracking of brain white matter fasciculi," *NeuroImage*, Vol. 12, pp. 184–195, 2000.

38. Coulon, O., D. Alexander, and S. R. Arridge, "Principal diffusion direction field regularisation for diffusion tensor magnetic resonance images," *Proc 9th Annual Meeting ISMRM, Glasgow*, p. 125, 1992.

39. Pajevic, S., A. Aldroubi, and P. J. Basser, "A continuous tensor field approximation of discrete DT-MRI data for extracting microstructural and architectural features of tissue," *J Magn Reson*, Vol. 154, pp. 85–100, 2002.

40. Wittenbrink, C. M., A. T. Pang, and S. K. Lodha, "Glyphs for visualizing uncertainty in vector fields," *IEEE Trans Visual Comput Graph*, Vol. 2, pp. 266–279, 1996.

41. Basser, P. J., "Quantifying errors in fibre-tract direction and diffusion tensor field maps resulting from MR noise," *Proc 5th Annual Meeting ISMRM, Vancouver*, Vol. 15, p. 1740, 1997.

42. Efron, B., "Bootstrap methods: another look at the jackknife," *Ann Statist*, Vol. 7, pp. 1–16, 1979.

43. Pajevic, S., and P. J. Basser, "Non-parametric statistical analysis of diffusion tensor MRI data using the bootstrap method," *Proc 7th Annual Meeting ISMRM, Philadelphia*, Vol. 15, p. 1790, 1999.

44. Hasan, K. M., D. L. Parker, and A. L. Alexander, "Bootstrap analysis of DT-MRI encoding techniques," *Proc 8th Annual Meeting ISMRM, Denver*, Vol. 15, p. 789, 2000.

45. Lazar, M., K. M. Hasan, and A. L. Alexander, "Bootstrap analysis of DT-MRI tractography techniques: streamlines and tensorlines," *Proc 9th Annual Meeting ISMRM, Glasgow*, p. 1527, 2001.

46. Mori, S., and P. C. M. van Zijl, "Fiber tracking: principles and strategies," *NMR Biomed*, Vol. 15, pp. 468–480, 2002.

47. Cheng, P., V. A. Magnotta, D. Wu, P. Nopoulos, D. J. Moser, J. Paulsen, R. Jorge, and N. C. Andreasen, "Evaluation of the GTRACT diffusion tensor tractography algorithm: A validation and reliability study," *NeuroImage*, Vol. 31, pp. 1075–1085, 2006.

48. Tournier, J. D., S. Mori, and A. Leemans, "Diffusion tensor imaging and beyond," *Magn Reson Med*, Vol. 65, no. 6, pp. 1532–1556, 2011.

49. Lazar, M., and A. L. Alexander, "White matter tractography using diffusion tensor deflection," *Human Brain Mapping*, Vol. 18, no. 4, pp. 306–321, 2003.

50. Lazar, M., and A. L. Alexander, "An error analysis of white matter tractography methods: synthetic diffusion tensor field simulations," *Neuroimage*, Vol. 20, pp. 1140–1153, 2003.

51. Lori, N. F., E. Akbudak, J. S. Shimony, T. S. Cull, A. Z. Snyder, R. K. Guillory, and T. E. Conturo, "Diffusion tensor fiber tracking of human brain connectivity: acquisition methods, reliability analysis and biological results," *NMR Biomed*, Vol. 15, no. 7-8, pp. 494–515, 2002.

52. Jones, D. K., "Challenges and limitations of quantifying brain connectivity in vivo with diffusion mri," *Imaging Med*, Vol. 2, pp. 341–355, 2010.

53. Jbabdi, S., and H. Johansen-Berg, "Tractography: Where do we go from here?," *Brain Connectivity*, Vol. 1, no. 3, pp. 169–183, 2011.

54. Mori, S., and P. B. Barker, "Mapping brain anatomical connectivity using white matter tractography," *NMR Biomed*, Vol. 23, pp. 821–835, 2010.

55. Chung, H. W., M. C. Chou, and C. Y. Chen, "Principles and limitations of computational algorithms in clinical diffusion tensor MR tractography," *AJNR Am J Neuroradiol*, Vol. 32, pp. 3–13, Jan 2011.

56. Bjornemo, M., "White matter fiber tracking using diffusion tensor MRI," Master's thesis, Linkoping University, Linkoping, 2002.

57. Jones, D. K., M. A. Horsfield, and A. Simmons, "Optimal strategies for measuring diffusion in anisotropic systems by magnetic resonance imaging," *Magnetic Resonance in Medicine*, Vol. 42, pp. 515–525, 1999.

58. Watts, R., C. Liston, S. Niogi, and A. M. Uluğ, "Fiber tracking using magnetic resonance diffusion tensor imaging and its applications to human brain development," *Mental retardation and developmental disabilities research reviews*, Vol. 9, no. 3, pp. 168–177, 2003.

59. Mang, S. C., D. Logashenko, D. Gembris, G. Wittum, W. Grodd, and U. Klose, "Diffusion simulation-based fiber tracking using time-of-arrival maps: a comparison with standard methods," *MAGMA*, Vol. 23, no. 5-6, pp. 391–398, 2010.

60. Kohonen, T., *Self-Organizing Maps*, Berlin: Springer, 2001.

61. Kohonen, T., "The self-organizing map," *Proceedings of the IEEE*, Vol. 78, pp. 1464–1480, Sep 1990.

62. Ritter, H., "Self-organizing feature maps: Kohonen maps," in *Handbook of Brain Theory and Neural Networks*, pp. 846–851, Cambridge: MIT Press, 1995.

63. Deoni, S. C., D. K. Jones, A. Simmons, S. C. R. Williams, and M. A. Horsfield, "Generation of a common diffusion tensor imaging dataset," *Proceedings of the ISMRM workshop on methods for quantitative diffusion methods for quantitative diffusion MRI of human brain*, 2005.

64. Wang, R., T. Benner, A. G. Sorensen, and V. J. Weeden, "Diffusion toolkit: A software package for diffusion imaging data processing and tractography," *Proc Intl Soc Mag Reson Med 15*, p. 3720, March 2007.

65. Wang, R., and V. J. Wedeen, *TrackVis.org*, Massachusetts General Hospital: Martinos Center for Biomedical Imaging.

66. Bihan, D. L., and P. van Zijl, "From the diffusion coefficient to the diffusion tensor," *NMR in Biomedicine*, Vol. 15, pp. 431–434, 2002.

67. Wirth, N., *Algorithms and Data Structures*, NJ, USA: Prentice-Hall, Inc., 1986.

68. Bihan, D. L., J. F. Mangin, C. Poupon, C. A. Clark, S. Pappata, N. Molko, and H. Chabriat, "Diffusion tensor imaging: Concepts and applications,"

69. Qin, C., N. Kang, and N. Cao, "Performance evaluation of anisotropic diffusion simulation based tractography on phantom images," *Proc of the 45th Annual Southeast Regional Conference (ACM-SE 45)*, pp. 521–522, 2007.